EMBRY-RIDDLE
Aeronautical University™
SCHOLARLY COMMONS

Dissertations and Theses

8-2014

Investigation of Traditional and Alternate Living Hinge Designs for Fused Deposition Modeling Additive Manufacturing Process

Cassandra Sue Gribbins

Scholarly Commons Citation

INVESTIGATION OF TRADITIONAL AND ALTERNATE LIVING HINGE DESIGNS FOR FUSED DEPOSITION MODELING ADDITIVE MANUFACTURING PROCESS

by

Cassandra Sue Gribbins

A Thesis Submitted to the College of Engineering Department of Mechanical Engineering in Partial Fulfillment of the Requirements for the Degree of Master of Science in Mechanical Engineering

Embry-Riddle Aeronautical University
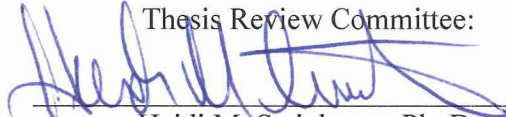Daytona Beach, Florida
August 2014

INVESTIGATION OF TRADITIONAL AND ALTERNATE LIVING HINGE
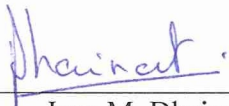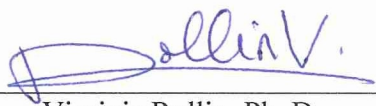DESIGNS FOR FUSED DEPOSITION MODELING ADDITIVE MANUFACTURING
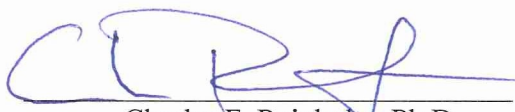PROCESS

by

Cassandra Sue Gribbins

This thesis was prepared under the direction of the candidate's Thesis Committee Chair,
Dr. Heidi M. Steinhauer, Professor, Daytona Beach Campus, and Thesis Committee
Members Dr. Jean M. Dhainaut, Professor, Daytona Beach Campus,
and Dr. Virginie Rollin, Professor, Daytona Beach Campus, and
has been approved by the Thesis Committee. It was submitted to the
Department of Mechanical Engineering in partial
fulfillment of the requirements for the degree of
Master of Science in Mechanical Engineering
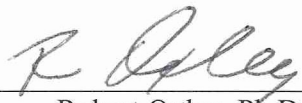
Thesis Review Committee:

Heidi M. Steinhauer, Ph. D.
Committee Chair

Jean M. Dhainaut, Ph. D.
Committee Member and
Graduate Program Chair,
Mechanical Engineering

Virginie Rollin, Ph. D.
Committee Member

Charles F. Reinholtz, Ph.D.
Department Chair,
Mechanical Engineering

Robert Oxley, Ph.D.
Associate Vice President of Academics

8-28-2014
Date

ii

Acknowledgements

Abstract

Researcher: Cassandra Sue Gribbins

Title: Investigation of Traditional and Alternate Living Hinge Designs for Fused
              Deposition Modeling Additive Manufacturing Process

Institution: Embry-Riddle Aeronautical University

Degree: Master of Science in Mechanical Engineering

Year: 2014

A manuscript-style thesis composed of three studies covered the application of living hinge designs in the additive manufacturing process of fused deposition modeling. Initial research included comparing numerical and analytical linear analyses on a traditional living hinge design. The second research consisted of tensile testing for the material properties of the Acrylonitrile Butadiene Styrene (ABS) used in fused deposition modeling (FDM) process by the MakerBot 2X as well as adjusting the traditional design to be printed. The third study explored alternate living hinge designs that utilize the geometric freedom provided by additive manufacturing to more evenly distribute stress across the hinge. The traditional living hinge design is not feasible for FDM ABS while alternate designs such as a longer hinge length or wave pattern demonstrated minimal stress experienced across the hinge. Further research on optimizing alternate designs is encouraged.

Table of Contents

List of Tables

List of Figures

Chapter 1

Thesis Introduction

Living hinges are a special design feature that utilize flexural material to incorporate bending in a single piece without the need of additional joining parts. An example of a commonly encountered living hinge is a book cover (Banister, 1987). Traditionally, living hinges are fabricated by injection molding or coining process, but lately there has been increased exploration into creating hinges via additive manufacturing (AM). Rapid Prototyping (RP) has also been used to describe the AM technologies that fabricate parts by adding material in a layered process (Ian Gibson, Rosen, & Stucker, 2010).

This thesis implements traditional living hinge designs to additive manufactured parts, analyzes the stresses occurring during bending applications, and utilizes the design freedom of additive manufacturing to generate alternate design geometry. The first manuscript, *Comparison of Numerical and Analytical Solutions of an ABS Additively Manufactured Living Hinge*, analyzes a traditional injection molded living hinge geometry including modifications to material properties with respect to AM capabilities. The second manuscript, *Experimental Analysis on an Additively Manufactured ABS Living Hinge*, conducts tensile testing to obtain more appropriate material properties as well as evaluates the dimensional accuracy of AM fabricated living hinges. The final manuscript, *Exploration of Alternate Living Hinge Designs for Entry Level FDM Systems*, implements alternate design geometry for living hinges and compares the printed dimensional accuracy between the fabricated AM parts.

Significance of the Study

Wohlers Report 2013 (Wohlers & Wohlers Associates, 2013) states that material extrusion systems are the largest base process of additive manufacturing machines. An entry level material extrusion company, MakerBot Industries, is the most popular 3D-printing company, and as of 2012 has sold more than 13,000 units (Wohlers & Wohlers Associates, 2013).

Entry level printers that sell for under $5,000 have shown a 346% growth in number of products sold each year from 2008 to 2011 (Wohlers & Wohlers Associates, 2013). Hobbyists, K-12 schools, engineering students, and "do-it-yourselfers" are cited as the market base for this level of machines. Though in recent years with the improvement in technology, companies like Ford Motor Company have started providing these entry level printers to their engineers for early concept design (Wohlers & Wohlers Associates, 2013).

Traditionally, additive manufacturing has been used to develop prototypes for concept verification and demonstration, but now the focus is broadening to also include the manufacture of production parts (Vaughan & Crawford, 2013).

Statement of the Problem

Currently, there is limited research on the application of living hinges in fused deposition modeling. Hinges that have been AM fabricated are not as durable as injection molded living hinges, but changes in design could help improve their durability. With the rise of entry level additive manufacturing machines, the need for establishing best design practices also increases.

Purpose Statement

The purpose of this study is to investigate the application of traditional living hinge design in additive manufacturing. This research is divided into three components. The first compares numerical and analytical solutions for an Acrylonitrile Butadiene Styrene (ABS) living hinge with respect to material property modifications governed by the guidelines for the fused deposition modeling process. The second conducts material testing along with fabrication of the traditional design for analysis on dimensional accuracy. The third explores the fabrication and analysis of alternate living hinge designs.

Assumptions

For the FEA cases, the application of a vertical enforced displacement was assumed to be analogous to a rotational displacement. The exclusion of the horizontal component and its effect on strain is noted for future research.

Chapter Two: *Comparison of Numerical and Analytical Solutions of an ABS Additively Manufactured Living Hinge*

Living hinges are commonly referred to as integral hinges and a type of flexure bearing. With proper design and construction, plastic hinges have been tested to flex more than a million cycles without failure (Kim, Son, & Im, 2003; Stratasys, Ltd., 2013). Living hinges are composed of a thin portion of material connecting two thicker walls with the main geometric features of an offset/recess and arc as illustrated in Figure 1.1.
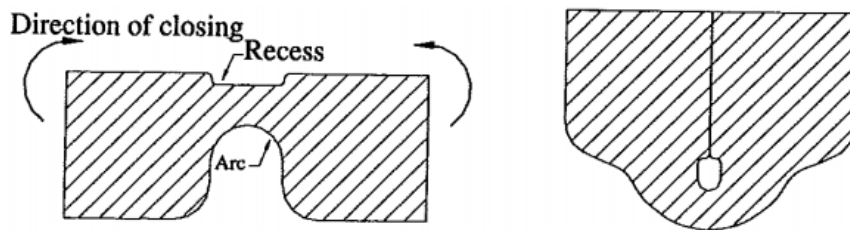
Figure 1.1 A common living hinge design illustrating major geometric design features and the result of bending 180° (Tres, 2000)

The recess in the upper portion, of Figure 1.1, is included to help prevent cracking and the arc in the lower portion orients the molecules to flex properly (Tres, 2000). Living hinges are also described as a compliant mechanism, a device that transfers motion through flexing members versus an assembly of rigid-bodies linked together (Howell, 2001). The bending of a living hinge is analogous to the pivoting of rigid-body pin joints except rotation is achieved through deflection of the flexible thin section of the hinge. Visual comparisons between the two assemblies are shown in Figure 1.2 where image A is the rigid-body assembly and image B is the living hinge.
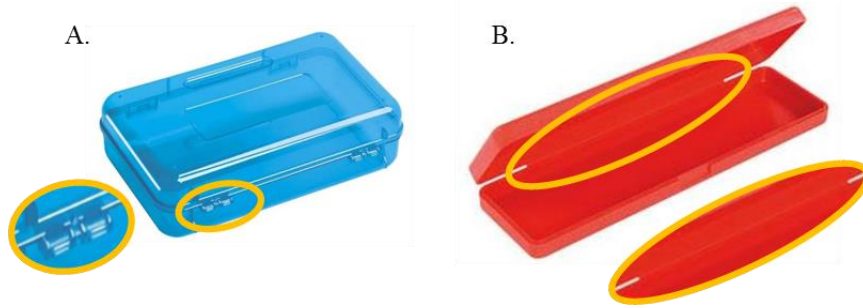
Figure 1.2 Plastic pencil case hinges: A. Rigid-body mechanical hinges and B. Living hinge

Across industries, an assembly of parts are typically more expensive than the manufacture of one part that incorporates a living hinge (Elleithy, 2007). In the automobile industry, living hinges have been used in electrical junction box covers. Figure 1.3 illustrates a part containing four living hinges (Kim et al., 2003).

Figure 1.3 Automobile electrical junction box cover containing four living hinges (Kim et al., 2003).

Living hinges are beneficial to micro electromechanical systems because of the minimal friction they produce (Stratasys, Ltd., 2013). One such application is programmable matter, which is a material whose physical properties can be programmed to change upon command (Knaian, 2013). A study by E. Hawkes et al. (2010) explored programmable matter, researchers utilized a living hinge design to implement

autonomous folding of an electronic sheet similar to origami paper folding shown in

Figure 1.4. The inclusion of multiple living hinges, as circled in B, allowed for the

bending of a single electronic sheet composed of multiple tiles instead of a complex set-

up with multiple subunits (Hawkes et al., 2010).
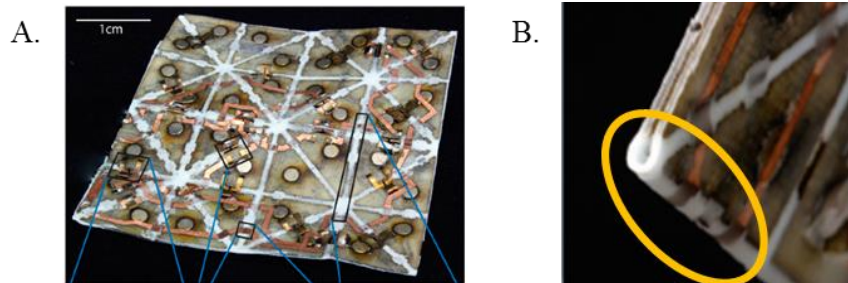
Figure 1.4 Electronic sheet with living hinge design: A. Overview of entire sheet containing 32 tiles connected by living hinges and B. Close-up of a single fold from a silicone flexure (Hawkes et al., 2010)

Consumer plastic products often incorporate living hinges as part of lidded

containers (Hoffman, 2004). An example of a consumer application is the top cover on a

Tic Tac mint case as shown in Figure 1.5.

Figure 1.5 Living hinge on a Tic Tac mint case (Objet Geometries Ltd., 2010)

6

The dimensions of a living hinge are derived by the material and type of application needed from the design. A traditional living hinge made out of polypropylene (PP) required to bend 180° as illustrated in Figure 1.1 (presented on page 4) would have the general dimensions as outlined in Figure 1.6 (Hoffman, 2004).
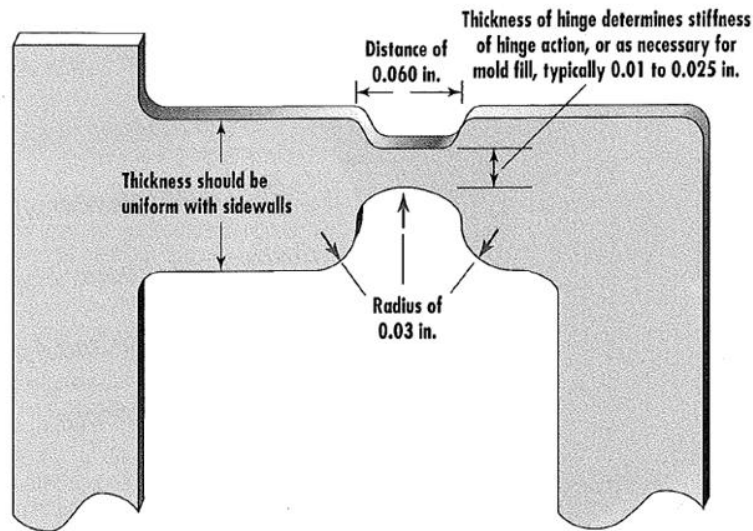
Figure 1.6 General dimensions for a polypropylene living hinge adapted from (Hoffman, 2004)

The traditional living hinge design was analyzed numerically and analytically. The numerical solution was obtained via CATIA's V5 R20 Finite Element Analysis (FEA) workbench. Paul A. Tres' *Designing Plastic Parts for Assembly* (2000) provided the framework for the analytical solution.

Chapter Three: *Experimental Analysis on an Additively Manufactured ABS Living Hinge*

Typically, plastic products incorporating living hinges are created by injection molding techniques (Hoffman, 2004). In injection molding, plastic pellets are melted and forced under high pressure into a mold. The melted plastic then takes the shape of the

mold, solidifies and is then ejected. Another process used is coining or cold working the part after it has been molded (Hoffman, 2004; Tres, 2000). This involves placing the part on a coining bed and having a heated die compress the section to plastically deform into the desired thickness.

Recently, other manufacturing processes – such as additive manufacturing (AM) – have been investigated for the fabrication of living hinges. AM technology consists of several different processes that produce parts from computer aided design (CAD) data. The creation of the parts is accomplished by creating a cross-section in the x-y plane and subsequently adding layer by layer in the z-direction to form a three-dimensional part (Ian Gibson et al., 2010).

Fused Deposition Modeling (FDM) is an extrusion based AM process. In FDM, material in a semi-solid state is guided through a nozzle to bond with previously extruded material as shown in Figure 1.7. The build plate is then lowered and the next cross-section is created on top of the previous layer (Ahn, Montero, Odell, Roundy, & Wright, 2002). This process can produce a part that has isotropic behavior in the x-y plane but anisotropic in the z-plane (Ian Gibson et al., 2010). This is due to the vertical layering of AM, typically strength in the z-direction of a part is less than the strength exhibited in the x-y plane (Ian Gibson et al., 2010).
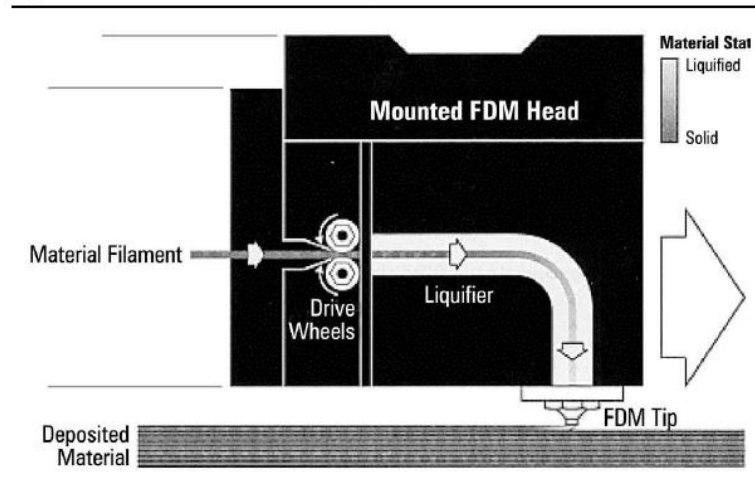
Figure 1.7 Diagram of the Fused Deposition Modeling Process (Ahn et al., 2002)

Tensile testing was performed to obtain applicable material properties for the

ABS used in the MakerBot 2X. The results were used to refine the FEA model of the

traditional living hinge design in CATIA V5 R20. Lastly, the printed dimensional

accuracy of the fabricated living hinge was also assessed as measured to nominal CAD

dimensions.

Chapter Four: *Exploration of Alternate Living Hinge Designs for Entry Level FDM Systems*

Stratasys, Ltd (2013), using proprietary material, has demonstrated that FDM

living hinges can last up to thousands of flex cycles. The special building considerations

were: a vertical build orientation and a hinge thickness of a single beadwidth.

The reduction in part count that living hinges offer is an important aspect for the

Design for Assembly (DFA) methodology which include guidelines for product

development (Poli, 2001). Design for Manufacturing (DFM) is a methodology that also

provides guidelines for developing part designs but with specific consideration to the

capabilities of manufacturing processes (Poli, 2001). For injection molding, an ideal part is ejected with as little tooling complexity as possible. Complex geometry containing features like undercuts could necessitate expensive moving parts within the die (Hague, Mansour, & Saleh, 2004).

DFM/DFA design guidelines suggesting minimizing part complexity do not impact additive manufacturing as greatly as other traditional manufacturing processes. With this lifted restraint of design complexity, reduction of part count by consolidating parts is more easily executable (Hague et al., 2004; Hopkinson, Hague, & Dickens, 2006).

This research investigated the effect of elongating the hinge length on the stress distribution during a bending application. Alternate geometry with complex designs were also explored to assess the effect on stress distribution. All alternate designs were fabricated with the MakerBot 2X using ABS, and printed dimensional accuracy was assessed.

Chapter Five: *Thesis Conclusion*

This chapter summarizes the findings from the initial numerical and analytical analysis, tensile testing, and fabrication of the living hinge designs. These findings provide guidance for designers looking to implement living hinge designs in additively manufactured parts. Suggestions for future work in further optimizing the application of living hinge designs are provided.

Definitions of Terms

Additive Manufacturing   A technology that consists of several different processes

    that produces parts from computer aided design (CAD) data

    layer by layer (Ian Gibson et al., 2010).

Design for Assembly   A methodology which include guidelines for product

    development (Poli, 2001).

Design for Manufacturing   A methodology that also provides guidelines for

    developing part designs with specific consideration to the

    capabilities of manufacturing processes (Poli, 2001).

Fused Deposition Modeling   An extrusion based AM process in which material in a

    semi-solid state is guided through a nozzle to bond with

    previously extruded material (Ian Gibson et al., 2010).

Rapid Manufacturing   An alternative term for Additive Manufacturing

    technologies (Hopkinson et al., 2006)

List of Acronyms

ABS	Acrylonitrile Butadiene Styrene
AM	Additive Manufacturing
AMUG	Additive Manufacturing Users Group
ASTM	American Society for Testing and Materials
CAD	Computer Aided Design
DFA	Design for Assembly
DFM	Design for Manufacturing
FDM	Fused Deposition Modeling
FEA	Finite Element Analysis
PP	Polypropylene
PE	Polyethylene
RM	Rapid Manufacturing
RP	Rapid Prototyping
SEM	Scanning Electron Microscope
SFF	Solid Freeform Fabrication

References

Ahn, S.-H., Montero, M., Odell, D., Roundy, S., & Wright, P. K. (2002). Anisotropic material properties of fused deposition modeling ABS. *Rapid Prototyping Journal*, *8*(4), 248–257.

Banister, R. A. (1987, July 23). Designing hinges that live. *Machine Design*, *59*(17), 103–106.

CES EduPack 2013. (2013). Polypropylene (PP). Granta Design Limited.

Elleithy, R. H. (2007). Plastic integral hinges; design, processing, and failure analysis. In *ANTEC 2007* (Vol. 5, pp. 2741–2744). Cincinnati, Ohio.

Gibson, I., Goenka, G., Narasimhan, R., & Bhat, N. (2010). Design Rules for Additive Manufacture. In *International Solid Freeform Fabrication Symposium An Additive Manufacturing Conference* (Vol. 2010, pp. 705–716). Austin, Texas: The University of Texas at Austin.

Gibson, I., Rosen, D. W., & Stucker, B. (2010). *Additive manufacturing technologies rapid prototyping to direct digital manufacturing*. New York; London: Springer. Retrieved from http://dx.doi.org/10.1007/978-1-4419-1120-9

Hague, R., Mansour, S., & Saleh, N. (2004). Material and design considerations for Rapid Manufacturing. *International Journal of Production Research*, *42*(22), 4691–4708.

Hawkes, E., An, B., Benbernou, N. M., Tanaka, H., Kim, S., Demaine, E. D., … Wood, R. J. (2010). Programmable matter by folding. *Proceedings of the National Academy of Sciences*, *107*(28), 12441–12445. doi:10.1073/pnas.0914069107

Hoffman, J. M. (2004, August 19). Care and feeding of living hinges. *Machine Design*, *76*(16), 64, 66.

Hopkinson, N., Hague, R. J. M., & Dickens, P. M. (2006). *Rapid manufacturing: an industrial revolution for the digital age*. Chichester, England: John Wiley.

Howell, L. L. (2001). *Compliant Mechanisms*. New York: John Wiley & Sons, Inc.

Kim, H. S., Son, J. S., & Im, Y. T. (2003). Gate location design in injection molding of an automobile junction box with integral hinges. *Journal of Materials Processing Technology*, *140*, 110–115. doi:10.1016/S0924-0136(03)00700-3

Knaian, A. N. (2013). Programmable matter. *Physics Today*, *66*(6), 64–65. doi:10.1063/PT.3.2020

Objet Geometries Ltd. (2010). Living Hinges. Retrieved from
     http://oldsite.objet.com/Portals/0/docs2/Applications_Connex/Living%20Hinges_
     Letter.pdf

Poli, C. (2001). *Design for manufacturing a structured approach*. Boston: Butterworth-
     Heinemann.

Stratasys, Ltd. (2013). Functional Prototyping - Living Hinges. Retrieved from
     http://www.stratasys.com/applications/functional-prototyping/living-hinges

Tres, P. A. (2000). *Designing Plastic Parts for Assembly* (4th ed.). Cincinnati: Hanser-
     Gardner.

Vaughan, M. R., & Crawford, R. H. (2013). Effectiveness of virtual models in design for
     additive manufacturing: a laser sintering case study. *Rapid Prototyping Journal*,
     19(1), 11–19.
     doi:http://dx.doi.org.ezproxy.libproxy.db.erau.edu/10.1108/13552541311292682

Wohlers, T. T., & Wohlers Associates. (2013). *Wohlers report 2013: additive
     manufacturing and 3D printing state of the industry : annual worldwide progress
     report*.

Chapter 2

Comparison of Numerical and Analytical Solutions of an ABS Additively Manufactured Living Hinge

Cassandra S. Gribbins

Embry-Riddle Aeronautical University

This article was presented at the Additive Manufacturing Users Group (AMUG) Conference in Tucson, Arizona on April 9th, 2014 and would document the results of analyzing a traditional and adjusted living hinge design.

"In many thermoplastic part designs, it is advantageous to create integral connecting members between parts that undergo relative movement, or for parts to be made in one tool and then assembled" (Tres, 2000, p. 178).

Abstract

This paper presents a comparison between numerical and analytical solutions of an additively manufactured Acrylonitrile Butadiene Styrene (ABS) living hinge. An introduction into the general design and use of living hinges is provided, followed by the approach used to determine the numerical and analytical solutions for a loading case where an enforced displacement is applied. A discussion of results is then presented. Lastly, a conclusion follows with an overview of possible future work. Through the work presented in this paper, it was concluded that although the analytical approach indicated a successful hinge, further experimental analysis is needed to support the findings of both numerical and analytical solutions.

Introduction

Living (also known as integral) hinges are a common design feature used in plastics. They utilize flexural material to incorporate bending in a single piece without the need of additional joining parts or assemblies. This is accomplished by having a relatively thin portion of material connecting two thicker walls (Tres, 2000). Living hinges can also be described as a compliant mechanism, a device that transfers motion through flexing members versus an assembly of rigid-bodies linked together (Howell, 2001). A hard book cover can be considered an example of a living hinge as the small section of decreased thickness between the front cover and side binding allows rotational movement (Banister, 1987).

The defining design geometry of living hinges is the thickness (2t), length (L_1), and offset/recess (l) as illustrated in Figure 2.1a. The hinge length, L_1, is measured as the length of the neutral axis in the center of the section. During bending, a recess in the upper portion is utilized to help prevent cracking by guiding bending of the material while an arc in the lower portion further encourages proper flexing, both of which are shown in Figure 2.1b.

The traditional design for most plastics is shown in a neutral flat position in Figure 2.1a and then in a 180 degree closing angle in Figure 2.1b. The direction of closing is upwards to enclose the recessed geometry. Other notable geometry like hinge radius (R) and length of the outer lower fiber (L_0) are shown in Figure 2.1b. The dimensions are a function of the chosen material's properties (Tres, 2000).

17
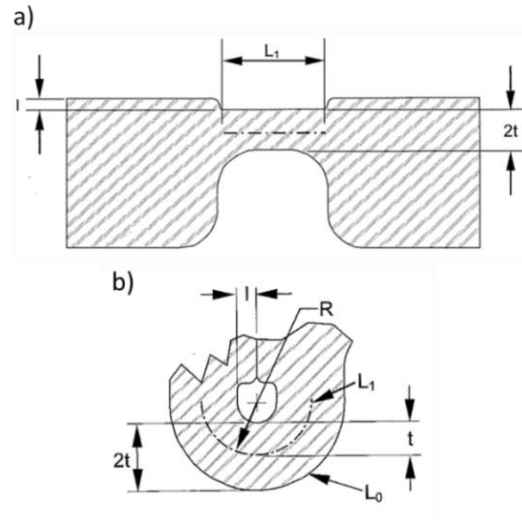
Figure 2.1 Defining design geometry for a living hinge in the a) opened position and b) closed position (Tres, 2000)

A living hinge can present a possible cost savings as it is one continuous part opposed to manufacturing multiple parts (Elleithy, 2007). A reduction in assembly considerations is another benefit of minimizing part count. In the automobile industry, living hinges have been used in electrical junction box covers as shown in Figure 2.2 (Kim, Son, & Im, 2003). The hinges act as built-in fasteners with a snap-fittings.

Figure 2.2 Automobile electrical junction box cover highlighting two sets of living hinges (Kim et al., 2003).

Plastic hinges are most common in consumer plastics as part of a lidded container (Hoffman, 2004). An example of a consumer application is the top cover on a Tic Tac mint case as shown in Figure 2.3.

Figure 2.3 Living hinge on a Tic Tac® mint case (Objet Geometries Ltd., 2010)

Polypropylene (PP) and polyethylene (PE) are most commonly used to produce living hinges due to their low material cost and high part lifecycle. The biggest benefit of using PP and PE is their excellent fatigue resistance. Hinges made of these two materials have their own optimized design geometry which is characterized by the complete arc at the bottom as shown in Figure 2.4c in the open position and the resultant closed form in Figure 2.4d. The lower portion on living hinges created with materials other than PP and PE utilize a design with an elongated width and radii-ed corners as shown for comparison in the neutral position in Figure 2.4a and the closed position in Figure 2.4b (Tres, 2000).
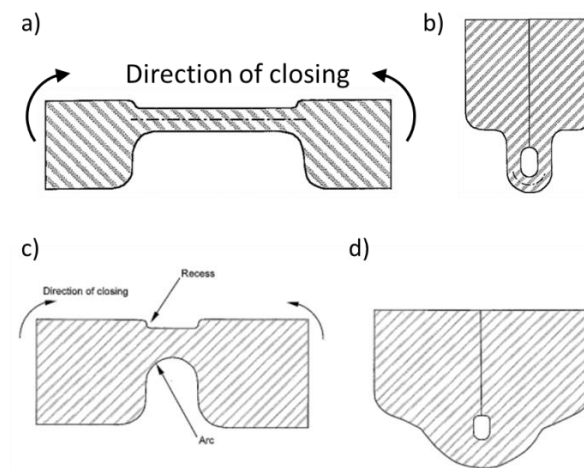
Figure 2.4 Types of living hinge designs: most engineering plastics a) open position and b) closed position, PP and PE a) opened and b) closed (Tres, 2000)

Typically, plastic products incorporating living hinges are created by injection molding techniques (Hoffman, 2004). In injection molding, plastic pellets are melted and forced under high pressure into a mold. The melted plastic then takes the shape of the mold, solidifies and then is ejected.

Another process used is coining or cold working the part after it has been molded (Hoffman, 2004; Tres, 2000). This involves placing the part on a coining bed and having a heated die compress the section to plastically deform into the desired thickness.

Recently, additive manufacturing (AM) has been explored to print living hinges. AM technology consists of several different processes that produces parts from computer aided design (CAD) data. The creation of the parts is accomplished by creating a cross-section in the x-y plane and subsequently adding layer by layer in the z-direction to form a three-dimensional part (Gibson, Rosen, & Stucker, 2010).

Fused Deposition Modeling (FDM) is an extrusion based AM process. In FDM, material in a semi-solid state is guided through a nozzle to bond with previously extruded material. This process can produce a part that is considered isotropic in the x-y plane but anisotropic in the z-plane (Gibson et al., 2010). Due to the vertical layering of AM, typically strength in the z-direction of a part is less than the strength exhibited in the x-y plane (Gibson et al., 2010).

The layering strategies and toolpath orientation of the part also affect the strength of the part. Rodriguez et al. (2001) performed an experimental investigation on the mechanical properties of FDM ABS as affected by fiber layout between each layer as well as within each layer. While moduli and strength were overall consistently lower for the FDM ABS compared to the monofilament stock material, the highest values for FDM

specimen consisted of aligned fibers between each layers as opposed to skewed layering. The higher values also resulted from specimen that overlapped the fibers within each layer (Rodríguez et al., 2001). A study by Ahn et al. (2002) also determines aligned layers and overlapping gaps results in higher strength. The tensile strength of FDM ABS varies from 65 to 72 percent that of injection molded ABS when fibers slightly overlap and layers alternate 90° (Ahn et al., 2002).

FDM living hinges have been demonstrated to last up to thousands of flex cycles by Stratasys, Ltd (2013) using the proprietary material Nylon 12. Special building considerations were a vertical build orientation and hinge thickness of a single beadwidth.

With proper design and construction, plastic hinges have been tested to flex more than a million cycles without failure under traditional injection molding techniques (Hoffman, 2004). Classification on what is considered part failure depends on whether the hinge is designed to experience only elastic strain or if plastic bending and/or tension is also permitted (Banister, 1987). If elastic strain is the defined limit, then plastic deformation would be considered failure of the part.

The maximum distortion energy theory is a commonly used failure theory for ductile materials under static loads (Howell, 2001; Lobontiu, 2003; Logan, 2007). This theory is also called the von Mises or von Mises-Hencky theory and compares von Mises stresses to the yield strength of the material. The von Mises stresses measure the intensity of the entire stress state in terms of three principal stresses or the x-y-z components (Logan, 2007). The three principal normal stresses are the maximum stresses in the three coordinate directions: σ_x, σ_y, and σ_z as illustrated in Figure 2.5 (Lobontiu, 2003).

21

The maximum shear stress or Tresca theory is another commonly used failure criterion of ductile materials under a static load. This theory categorizes failure as maximum shear stress equal to or greater than the tensile-test yield shear stress (Howell, 2001; Lobontiu, 2003).
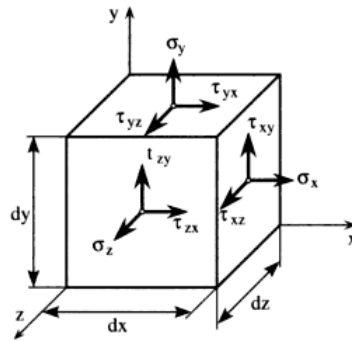
Figure 2.5 Three dimensional stress element (Lobontiu, 2003)

Technical Objective and Approach

The purpose of this research was to explore the application of a traditional design approach for living hinges in additive manufacturing. The objective of this analysis was to compare bending stresses evaluated from a numerical and analytical approach. For the numerical approach, the von Mises theory for evaluating stress was preferred over the Tresca theory as it has experimentally been shown to result in a slightly more accurate solution (Lobontiu, 2003). Furthermore, it is utilized in many finite-element computer programs. A widely used analytical approach, outlined by Paul A. Tres (2000), for designing and evaluating living hinges was used for comparison.

Access to a Makerbot 2X defined the material constraint to ABS for this study. While living hinges are more commonly produced using PP and PE, other materials have

been used. Through ABS is not known for its ductile nature, the other material option of polylactic acid (PLA) is too brittle.

The material properties of ABS needed for the analysis were obtained from CES EduPack (2013). As shown in the data sheet presented in Appendix A, there is a range of values for each property. For the purpose of this study, the averages for the ranges of the necessary material properties were used.

As there is limited data published for additively manufactured materials, the CES EduPack 2013 defined tensile strength for injection molded ABS was reduced to 65% for the purpose of this study. In Ahn et al.'s study (2002) on the anisotropic material properties of fused deposition modeled ABS they found that FDM ABS had 65-72% tensile strength of injection molded plastic. Therefore, the analysis used the conservative 65% of the tensile strength for the evaluation of the living hinges which is 28.6 MPa.

Two sets of design geometry were used in the research. A traditional polypropylene design as shown in Figure 2.4 and an adjusted design with respect to additive manufacturing recommendations. The traditional polypropylene design was used as general measurements for the 'all other plastics' design were not found. The second design geometry consisted of only a modified hinge thickness with respect to the additively manufacturing guideline of keeping the thickness of a part an integer function of the machine nozzle width (Ahn et al., 2002). Isolating the thickness also allows for observation on any effect of strain experienced.

A displacement of 10° and 45° for each design geometry was conducted. The 10° adheres to maximum deformation under linear computational guidelines and 45° offers a more realistic application situation.

CATIA V5 R20 was used to provide numerical solutions to the finite element model. The load case consisted of having a fixed constraint on one end of the part while the other end was subjected to an enforced displacement. While plastic behavior is nonlinear, the workbenches available in CATIA V5 R20 allowed for linear computation. This was acceptable as the analytical equations are also linear which offer a fair comparison between the two results.

Due to the linear computation constraint, only a fully elastic hinge design can be assessed. Determination of a successful plastic hinge would require non-linear analysis or experimental study.

Related Theory

The analytical approach, adapted from Paul A. Tres (2000), is outlined in Appendix B. The defining dimensions of hinge recess, thickness, and length are identified first and then assessed to determine the type of strain experienced by the hinge. Case A is associated with elastic bending. Case B is general plastic bending while Case C evaluates pure plastic bending and Case D evaluates a mixture of plastic bending and tension.

An example of a stress-strain curve for a ductile thermoplastic is shown in Figure 2.6. The figure is proportionally similar to experimental curves of ABS (Rodríguez et al., 2001). Assessing hinge behavior begins by evaluating if bending results in strain under the yield point and within the elastic region. Beyond the yield point the hinge will permanently deform within the plastic region until the point of rupture (Howell, 2001).
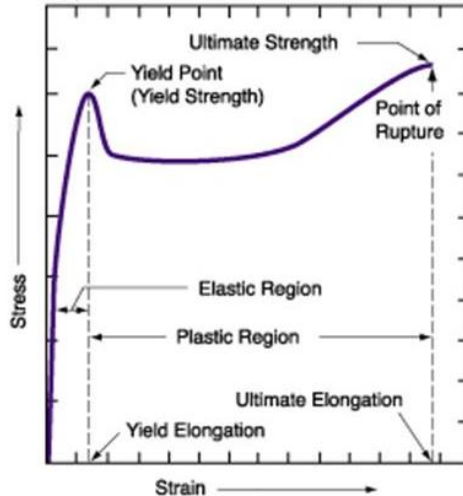
Figure 2.6 Typical stress-strain curve for a ductile thermoplastic (Patterson, n.d.)

When designing for a fully elastic hinge, failure is defined as bending stress equal to the material's yield strength, establishing any yielding of the part as failure. Whereas a fully plastic hinge defines failure as bending strain equal to the ultimate strain of the material resulting in fracture of the part (Banister, 1987; Tres, 2000).

The case of elastic bending is illustrated in Figure 2.7. When considering the overall thickness as outlined in Figure 2.7a, the strain distribution is linearly approximated in Figure 2.7b. Strain will be at its maximum on the outer layers of the overall hinge thickness. Considering that the hinge closes upwards, the top layer will be in compression as shown with the negative strain and the lower layer in tension as indicated by positive strain in the diagram (Banister, 1987).
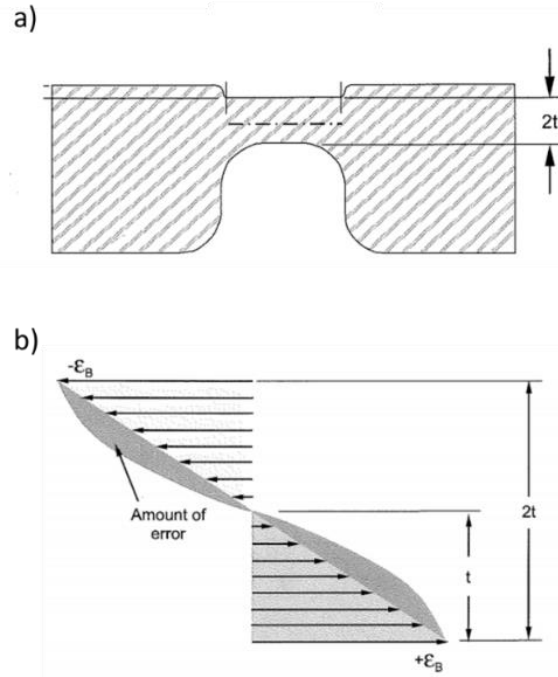
Figure 2.7 Purely elastic strain case considering a) overall width of the hinge for b) linear approximation of strain distribution (Tres, 2000)

The calculations to determine if the chosen hinge length will only experience strain within the elastic region consists of the assumptions that the hinge bends in a 180° circular closing path and that the neutral axis in located in the center of the hinge. Equation 2.1 represents these assumptions with the length of the neutral axis, L_1, equal to π multiplied by the hinge radius, R.

$$L_1 = \pi R \tag{2.1}$$

The length of the lower fiber can be written in terms of the hinge radius, R, half of the hinge thickness, t, and π. This relation is shown in Equation 2.2.

$$L_0 = (R + t)\pi \tag{2.2}$$

Bending strain, $\varepsilon_{BENDING}$, can be written as a function of the change in length of the lower fiber, L_0, over the neutral axis, L_1. Substituting and simplifying the relation results in bending strain equal to half the hinge thickness, t, divided by the hinge radius, R, as shown in Equation 2.3.

$$\varepsilon_{BENDING} = \frac{t}{R} \tag{2.3}$$

Rearranging Equation 2.1 for hinge radius, R, and substituting into Equation 2.3 results in bending strain, $\varepsilon_{BENDING}$, equal to π multiplied by half the hinge thickness divided by the neutral axis as shown in Equation 2.4.

$$\varepsilon_{BENDING} = \frac{\pi t}{L_1} \tag{2.4}$$

To meet the condition of a fully elastic hinge, the bending stress is to be less than the yield strength of the material. Using Hooke's law to relate the bending strain to bending stress, $\sigma_{BENDING}$, is shown in Equation 2.5, where E is the Young's modulus of the material.

$$\sigma_{BENDING} = E\,\varepsilon_{BENDING} \tag{2.5}$$

To apply the condition of a fully elastic hinge, the equation turns into an inequality replacing bending stress with the yield strength, σ_{YIELD}, of the material. The bending strain is substituted with Equation 2.4. Reordering the inequality for the length

of the neutral axis, L_1, provides the minimum length as shown in Equation 2.6. Condition A referenced in the algorithm presented in Appendix B is the right side of the equation.

$$L_1 > \frac{\pi t E}{\sigma_{YIELD}} \tag{2.6}$$

If the chosen length of the hinge is less than the condition in Equation 2.6, then plastic analysis will be required. A hinge length satisfying Equation 2.6 indicates that the hinge is in elastic bending and the analysis can be stopped. A plastic hinge can either experience pure bending strain for a mixture of bending and tension.

For the pure bending case, the minimum hinge length is the hinge recess depth, l, plus half of the hinge thickness, t, and multiplied by π as shown in Equation 2.7. Condition B referenced in the algorithm presented in Appendix B is the right side of the equation.

$$L_1 > \pi(t + l) \tag{2.7}$$

If the chosen hinge length satisfies the inequality, then the hinge is experiencing pure bending. To determine if the hinge will fail, Equation 2.6 is rewritten in terms of ultimate strain, $\varepsilon_{ULTIMATE}$, or the point of rupture in the hinge. This condition is shown in Equation 2.8 with the right side referencing Condition C from Appendix B. Violating the inequality indicates failure.

$$L_1 > \frac{\pi t}{\varepsilon_{ULTIMATE}} \tag{2.8}$$

When the chosen hinge length violates the inequality from Equation 2.7, the hinge behaves like a viscoelastic material experiencing a necking effect from a combination of bending and tension. To determine if the hinge will fail, the condition for the minimum hinge length is determined from the inequality of strain from tension, $\varepsilon_{TENSION}$, plus strain from bending, $\varepsilon_{BENDING}$, and less than ultimate strain, $\varepsilon_{ULTIMATE}$, as shown in Equation 2.9.

$$\varepsilon_{TENSION} + \varepsilon_{BENDING} < \varepsilon_{ULTIMATE} \qquad (2.9)$$

Strain from tension and bending are derived from geometrical lengths that account for the necking behavior experienced in the plastic region before the hinge ruptures and fails. The calculation for the length of the lower fiber is expanded to include the change in length due to the necking effect. Length of the lower fiber is equal to π multiplied by the recess radius in the closed position due to necking effects, l', in addition to the hinge radius in the closed position due to necking effects, $2t'$ as shown in Equation 2.10.

$$L_0 = \pi(l' + 2t') \qquad (2.10)$$

The strains due to bending and tension are related to the modified calculation for the length of the lower fiber of the hinge. This relation includes the introduction of Poisson's ratio, ν, which relates the strain in the longitudinal direction to the strain in the

transverse direction. Therefore, the change in hinge thickness is related to strain due to

tension as shown in Equation 2.11.

$$\Delta t = 2t\nu\varepsilon_{TENSION} \tag{2.11}$$

Relating strain from tension to the bending strain can then be obtained. Equation

2.12 illustrates the modified calculation for bending strain with respect to necking effects.

$$\varepsilon_{BENDING} = \frac{\pi}{L_1}(t - t\nu\varepsilon_{TENSION}) \tag{2.12[1]}$$

Rearranging and combining Equation 2.11 and Equation 2.12 to obtain the left

side of the inequality in Equation 2.9 can be used to establish the minimum neutral length

condition for a hinge experiencing both tension and bending.

This condition is shown in Equation 2.13 with the right side referencing

Condition D from Appendix B. Violating the inequality indicates failure.

$$L_1 > \frac{\pi\nu(2t+l)}{\nu + 2\left(1 - \sqrt{1 - \nu\varepsilon_{ULTIMATE}}\right)} \tag{2.13}$$

---

[1] A detailed derivation can be found in Chapter 7 on Living Hinges in Paul A. Tres' *Designing Plastic Parts for Assembly* (2000).

Experiments

The geometry used for the initial analysis was the traditional PP design geometry as shown in Figure 2.8a as dimensions for the general design of all other plastics are not established.

The numerical analysis using CATIA V5 R20 consisted of creating a solid model. The base sketch of the model is shown in Figure 2.8b with the final solid model shown in Figure 2.8c.
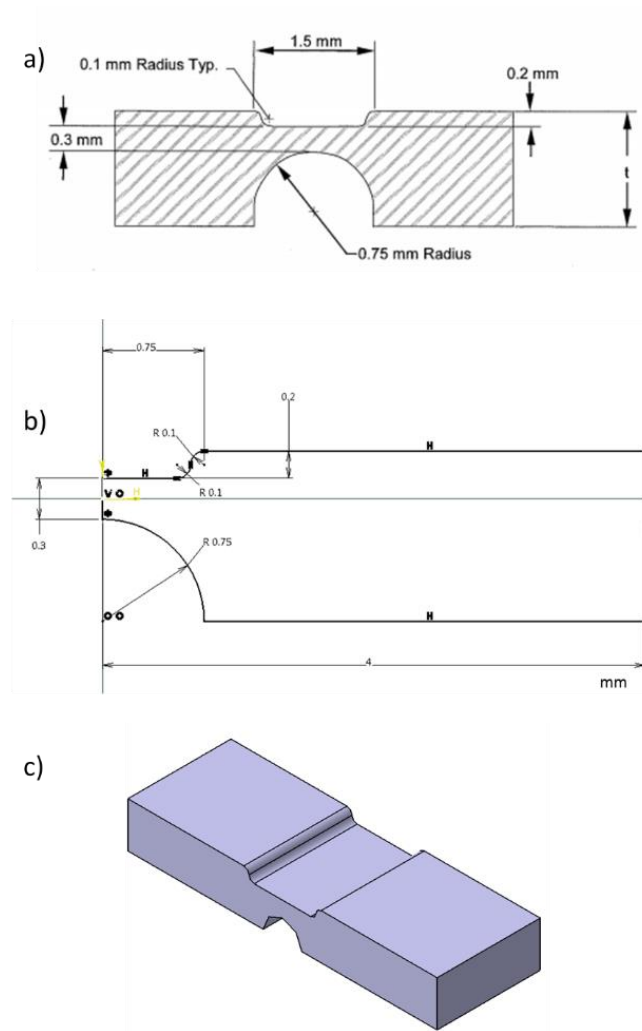
Figure 2.8 Traditional PP design geometry analysis: a) referenced geometry (Protomold, 2007; Tres, 2000), b) CATIA V5 R20 base sketch, and c) CATIA V5 R20 isometric view of complete solid model

Material properties of ABS were applied to the solid model. While an anisotropic material option was present to define the material type, there were many required fields where data was not available as shown in Figure 2.9. Therefore, all cases were conducted with isotropic material applied to the solid part. The completed material property option is shown in Figure 2.10 references values provided in Appendix A from CES EduPack (2013). The yield strength represents the reduced value of, 28.6 MPa, the reported average from CES EduPack 2013 with respect to estimated FDM material properties for ABS (Ahn et al., 2002).
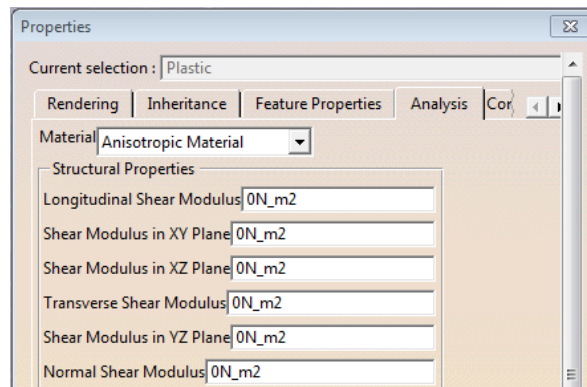
Figure 2.9 CATIA V5 R20 anisotropic material option

In the Generative Structural Analysis workbench, a static analysis case was chosen to base the analysis in a linear computation versus the other option for a frequency analysis. The options for the OCTREE Tetrahedron Mesh were left as the default to start as the program adjusts the size with respect to the solid model. The element type was selected to be parabolic rather than linear for a more accurate solution (Zamani, 2010). After running a solution, the mesh was refined to smaller sizes until the resultant maximum von Mises stress values varied less than three percent between cases.
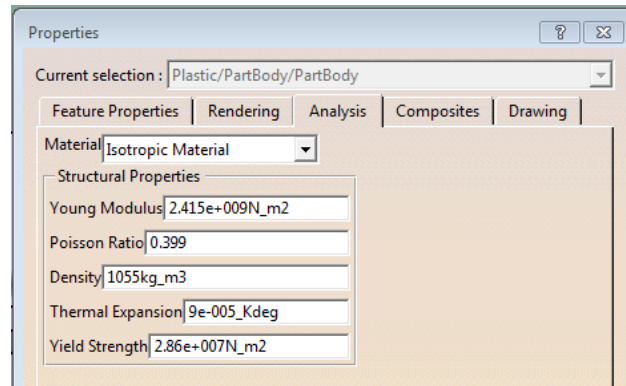
Figure 2.10 CATIA V5 R20 applied isotropic material properties

Boundary conditions for the model consisted of a fixed constraint and an enforced displacement. The leftmost surface was applied with a fixed constraint for movement restrictions of all translation and rotation on that surface.

A 10° rotation on the rightmost face was desired for the enforced displacement, but due to complications in applying a rotation command, a comparable vertical translation of 0.7mm was applied. For the 45° rotation, an analogous 4.0 mm vertical translation was applied. The horizontal component of the displacement was not included in the analysis. For a 10° rotation, the induced horizontal displacement would result in approximately 1% strain while the 45° rotation would result in approximately 30% strain. The inclusion of the effect of this high strain is a limitation on the study noted for future research.

The enforced displacements were related to move in reference to the coordinate system origin located in the center of the living hinge to encourage circular bending about the center of the hinge. Figure 2.11 illustrates the finite element model with the constraint and an enforced displacement applied.
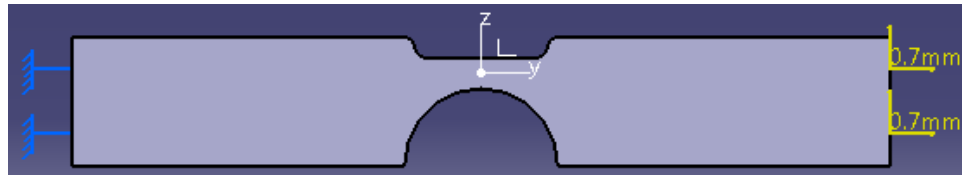
Figure 2.11 CATIA V5 R20 side view of living hinge finite element model with fixed constraint and enforced displacement of 0.7 mm in the positive Z direction

The analytical approach based on the algorithm shown in Appendix B was conducted with the use of MATLAB R2013a. The code is provided in Appendices C and D. The equations were adapted to take into account closing angles of 10° and 45°. When running the code, the user first inputs material then the defining geometric dimensions before running through the calculations to determine the type of strain the hinge is experiencing and whether the hinge will fail.

Table 2.1 shows the user input variables for the first analysis using the traditional PP design geometry shown in Figure 2.8a. The asterisk next to the material type reflects the adjusted material property profile containing the reduced yield strength. The processing thickness used within the code is half of the overall thickness as instructed by the algorithm from Paul A.Tres (2000).

Table 2.1 Analytical approach user input variables – traditional PP design geometry

User Input			
Material		ABS*	
Processing Thickness		0.15	mm
Hinge Length		1.3	mm
Hinge Recess		0.2	mm
Closing Angle		10, 45	deg

34

The second analysis utilized a modified geometry with respect to additive manufacturing guidelines that recommends a thickness as a function of the nozzle diameter (Ahn et al., 2002). The Makerbot 2X's nozzle diameter of 0.1 mm defined a minimum allowable hinge thickness.

The CATIA V5 R20 sketch was updated to include the change in geometry as shown in Figure 2.12 with the modified thickness highlighted.
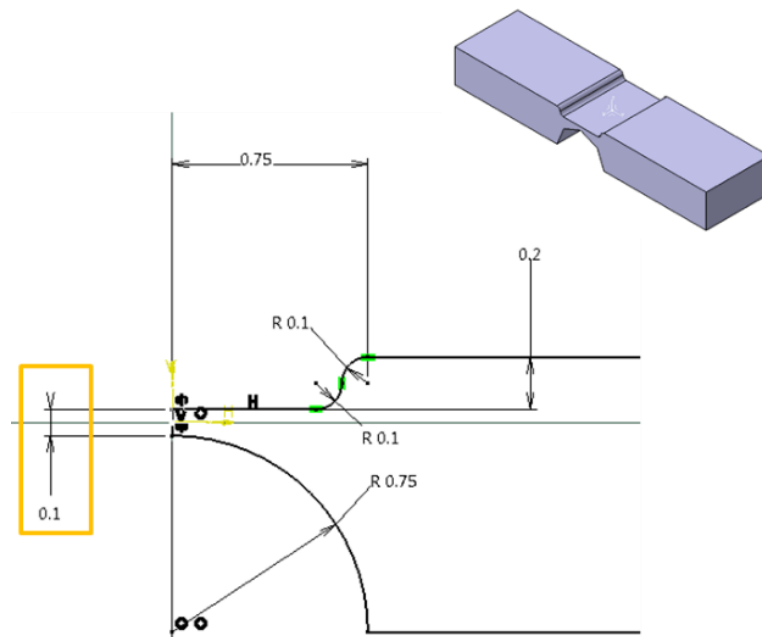
Figure 2.12 Adjusted AM design geometry CATIA V5 R20 base sketch and isometric view of complete solid model highlighting change in thickness

Table 2.2 shows the user input values used in the analytical approach highlighting the change in processing thickness.

Table 2.2 Analytical approach user input variables - adjusted AM design geometry

User Input			
Material		ABS*	
Processing Thickness		0.05	mm
Hinge Length		1.3	mm
Hinge Recess		0.2	mm
Closing Angle		10, 45	deg

Results and Discussion

Table 2.3 displays the results of the numerical and analytical analyses with both closing angle cases of 10° and 45°. Under the elastic case, failure criteria is taken as bending stress higher than the yield strength of 28.6 MPa.

The first analysis of the traditional PP design with a hinge thickness of 0.3 mm had an enforced displacement of 0.7 mm. The translational diagram shown in Figure 2.13 verifies that the hinge deformed as desired with the left side stationary and motion occurring about the center of the hinge. A larger image of the displacement diagram is shown in Figure E-1 under Appendix E. The slight increase in the maximum displacement of 0.714 mm can be attributed to how CATIA V5 R20 handles forced translation on the surface and where it chose to take the reference point of the surface. The resultant von Mises stress for 73.52 MPa is beyond the yield strength indicating hinge failure under the numerical approach.

The analytical approach indicated a hinge behavior of pure plastic bending and bending stress of 48.60 MPa which, although lower than the numerical approach, also exceed the yield strength. The difference between the two analyses is 33.80%.
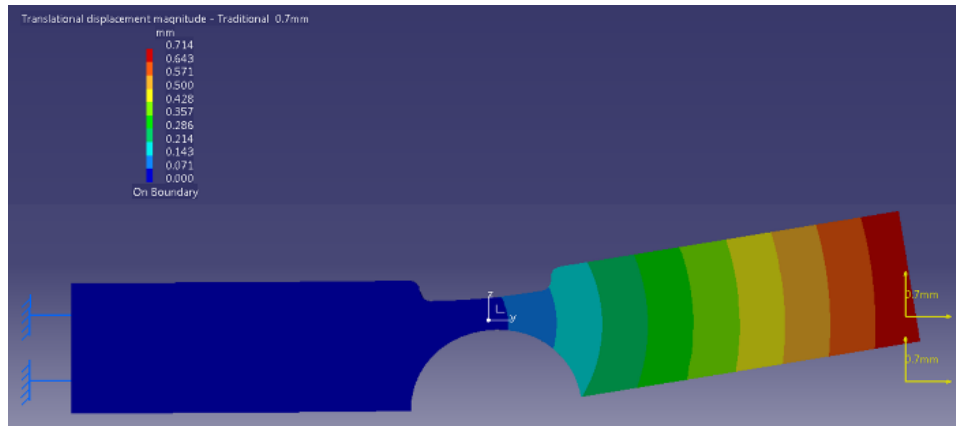
Figure 2.13 Translational displacement vector diagram for traditional PP design geometry with an enforced displacement of 0.7 mm

The translational displacement diagram for the increased closing angle of 45°

again verified the correct deformation, albeit with a higher maximum displacement of

4.08 mm. The translational displacement diagram is shown in Figure F-1 under Appendix

F.

Both the von Mises and bending stress for the increased closing angle of 45°

result in stresses (420.12 MPa and 218.90 MPa, respectively) that exceed the yield

strength. The percent difference between the results is 47.90%. Pure plastic bending was

again indicated as occurring by the analytical approach.

Table 2.3 Results for Numerical and Analytical Approach for Traditional PP and Adjusted AM Design Geometry at Enforced Displacements of 0.7 mm and 4.0 mm

| | Hinge Thickness (mm) | Numerical Approach | | Analytical Approach | | | % Difference von Mises & Bending Stress |
		Enforced Displacement (mm)	von Mises (Mpa)	Closing Angle (deg)	Hinge Behavior	Bending Stress (Mpa)	
Traditional PP	0.15	0.7	73.52	10	Pure Plastic Bending	48.60	33.80
	0.15	4.0	420.12	45	Pure Plastic Bending	218.90	47.90
Adjusted AM	0.05	0.7	48.59	10	Pure Elastic	16.20	66.60
	0.05	4.0	277.65	45	Pure Plastic Bending	73.00	73.80

The stresses for the adjusted AM geometry were all smaller than their counterparts in the traditional PP geometry analysis, but all still exceeding the yield strength except for the 10° case under the analytical approach. The 10° case, indicated to be in pure elastic bending, resulted in 48.59 MPa for the von Mises stress in the numerical approach and 16.20 MPa for the bending stress in the analytical approach. The numerical approach for the 45° case resulted in 277.65 MPa and in the analytical approach, 73.00 MPa. Pure plastic bending is indicated for the 45° closing angle.

The higher experienced stresses reported by CATIA may be over-estimated as the analytical approach determined the hinge behaving within the plastic region. This would infer CATIA's inaccuracy with its solution since the analysis utilizes linear computation. The true values of stress experienced within the hinge would be between the conservative analytical results and the over-estimated CATIA results.

The percent difference between the numerical and analytical approach for both closing angles were higher than the differences within the traditional PP design geometry.

The closing angle of 10° resulted in 66.60% difference between stresses while the 45° case resulted in a 73.80% difference.

All of the stresses calculated from the analytical approach were smaller than the numerical approach values. This is expected as the analytical equations are more conservative. The difference between the stresses between the numerical and analytical approaches were relatively high. A difference between the approaches is expected as the analytical approach employs geometric assumptions of a constant cross-sectional area across the hinge. The greater differences in the adjusted AM stresses versus the traditional PP stresses can be attributed to the greater variance of cross-sectional area within the hinge. The radius on the lower portion of the hinge induces a variable cross-section across the hinge, as shown in Figure 2.8b for the traditional PP design and Figure 2.12 for the adjusted AM design. This variance is further accentuated with the smaller thickness in the Adjusted AM design. The analytical equations would be greatly affected by the change in area resulting in the higher difference as well as the difference in applied displacement.

Pure plastic bending was indicated by the analytical approach for both traditional PP geometry displacement cases as well as the adjusted AM 45° displacement case. Determining failure of the hinge would require comparison of experienced stress with the material's ultimate strength, which requires experimental data.

Figure 2.14 shows the stress distribution diagram under the numerical approach using CATIA V5 R20 for the traditional PP geometry case with a 10° displacement. The upper and lower portions of the hinge appear to have higher concentrations of stress. This

correlates with the highest tension and compression stresses occurring at the topmost and bottommost sections of the living hinge, further indicating a correct solid model setup.

CATIA V5 R20 displacement and stress diagrams are shown in Appendix E for the traditional PP geometry 10° case and Appendix F for the 45° case. Both adjusted AM geometry stress diagrams are shown in Appendix G.
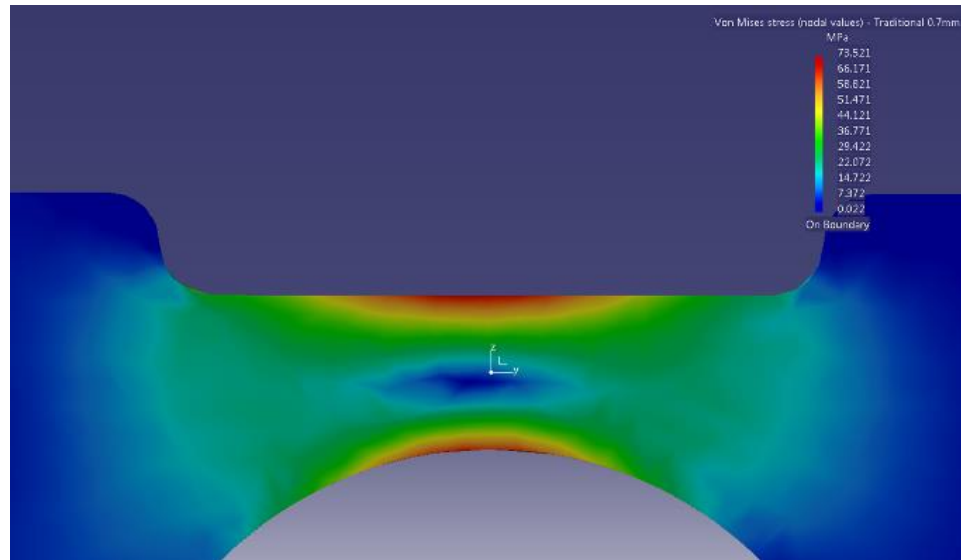
Figure 2.14 Von Mises stress diagram for enforced displacement 0.7 mm on traditional PP design geometry

Conclusions and Future Work

The numerical analysis using CATIA V5 R20 resulted in expected deformations and stress distributions as defined in the theory of living hinges. Comparing the calculated stresses with the yield strength to determine hinge failure showed that all but one case failing by indicating plastic behavior. Determination where the hinge fails within the plastic region requires further experimental work.

The value of the limiting yield strength for ABS also deserves more research. Ahn et al.'s study (2002) related the yield strength between injection molded and FDM ABS also described an issue during material testing. The common dogbone-shaped sample was prone to break at the radii because of the toolpath which created a stress concentration at the section. They in turn used a different standard for tensile testing which simplified the design to a straight rectangular shape (Ahn et al., 2002).

Future work would involve conducting material property testing for more accurate values to be used in the analyses as well as an FEA case that includes the effects for the horizontal displacement. Experimental data on the application of rotating the living hinge would help better understand and refine the method for conducting the numerical and analytical analyses.

References

Ahn, S.-H., Montero, M., Odell, D., Roundy, S., & Wright, P. K. (2002). Anisotropic material properties of fused deposition modeling ABS. *Rapid Prototyping Journal*, *8*(4), 248–257.

Banister, R. A. (1987, July 23). Designing hinges that live. *Machine Design*, *59*(17), 103–106.

CES EduPack 2013. (2013). Polypropylene (PP). Granta Design Limited.

Elleithy, R. H. (2007). Plastic integral hinges; design, processing, and failure analysis. In *ANTEC 2007* (Vol. 5, pp. 2741–2744). Cincinnati, Ohio.

Gibson, I., Rosen, D. W., & Stucker, B. (2010). *Additive manufacturing technologies rapid prototyping to direct digital manufacturing*. New York; London: Springer. Retrieved from http://dx.doi.org/10.1007/978-1-4419-1120-9

Hoffman, J. M. (2004, August 19). Care and feeding of living hinges. *Machine Design*, *76*(16), 64, 66.

Howell, L. L. (2001). *Compliant Mechanisms*. New York: John Wiley & Sons, Inc.

Kim, H. S., Son, J. S., & Im, Y. T. (2003). Gate location design in injection molding of an automobile junction box with integral hinges. *Journal of Materials Processing Technology*, *140*, 110–115. doi:10.1016/S0924-0136(03)00700-3

Lobontiu, N. (2003). *Compliant Mechanisms: design of flexure hinges*. Boca Raton: CRC Press LLC.

Logan, D. L. (2007). *A first course in the finite element method*. Toronto, Canada: Thomson.

Objet Geometries Ltd. (2010). Living Hinges. Retrieved from http://oldsite.objet.com/Portals/0/docs2/Applications_Connex/Living%20Hinges_ Letter.pdf

Patterson, T. (n.d.). *Typical Stress/Strain Curve for a Ductile Thermoplastic*. Retrieved from http://www.schenectady.k12.ny.us/users/pattersont/IBDT%20Website/Page_Gener ators/StressDuctileThermoplastic.html

Protomold. (2007, May). Design tips for rapid injection molding. Retrieved from http://www.protomold.com/design_tips/unitedstates/2007/2007-05_designtips/default.htm

Rodríguez, J. F., Thomas, J. P., & Renaud, J. E. (2001). Mechanical behavior of acrylonitrile butadiene styrene (ABS) fused deposition materials. Experimental

investigation. *Rapid Prototyping Journal*, *7*(3), 148–158. doi:10.1108/13552540110395547

Stratasys, Ltd. (2013). Functional Prototyping - Living Hinges. Retrieved from http://www.stratasys.com/applications/functional-prototyping/living-hinges

Tres, P. A. (2000). *Designing Plastic Parts for Assembly* (4th ed.). Cincinnati: Hanser-Gardner.

Zamani, N. G. (2010). *CATIA V5 FEA tutorials: release 19*. Mission, KS: SDC Publications.

Chapter 3

Experimental Analysis on an Additively Manufactured ABS Living Hinge

Cassandra S. Gribbins

Embry-Riddle Aeronautical University

This article was presented at the Solid Freeform Fabrication (SFF) Symposium in Austin, Texas on August 4th, 2014 and would detail tensile testing and fabrication of a traditional living hinge design. A portion of this research would be published in the Solid Freeform Fabrication Symposium Proceedings.

"FDM parts … are amongst the strongest AM polymer parts available, but when they are desired as a functional end-use part, this may mean they need substantial finishing … as they exhibit lower accuracy than some other AM technologies" (Ian Gibson, Rosen, & Stucker, 2010, p. 49).

Abstract

A study on the plastic behavior of an additively manufactured Acrylonitrile Butadiene Styrene (ABS) living hinge was conducted using a MakerBot 2X. Initial research included numerical and analytical linear analyses on a typical living hinge design. This paper introduces the portion of the research that explores the application of traditional design practices to entry-level additive manufacturing machines. Tensile testing for material properties was conducted to refine the numerical model. Experimental rotational testing was conducted for data on the non-linear, plastic behavior experienced during application. Verification of the numerical model with experimental results will be used to guide future work on exploring alternate design geometries that leverage the advantages of additive manufacturing's design freedom for smoother stress distribution on the hinge.

Introduction

Inducing flexural capabilities within a single plastic piece is often executed through the utilization of a living hinge design. Bending is achieved by creating a relatively thin section of plastic between two larger, rigid regions. Incorporating living hinges in a design reduces part count which can result in lower overall costs and assembly time (Tres, 2000).

Initial research compared numerical and analytical analyses of a traditionally design living hinge against an alternate design. There was a large percent difference between stresses from the two solutions due to the analytical solution being conservative and the numerical solution overestimating the non-linear results. The initial research also indicated the hinges behaving in the plastic region under a small deformation of 10°. Comparing the calculated stresses with the yield strength to determine hinge behavior showed that all cases acted within the plastic region under the enforced deformation.

Further research suggestions to refine the results included testing for more applicable material properties for analysis and failure criteria of the living hinge. The initial research adjusted the yield strength of bulk ABS with respect to experimental investigations from Ahn et al. (2002) and Rodriguez et al. (2001) that demonstrated fused deposition modeled (FDM) ABS having 65 to 75% yield strength of injection molded ABS, resulting in a usable yield strength of 28.6 MPa. In Ahn et al.'s study (2002) the common dogbone-shaped sample defined by the ASTM D638-10 standard was prone to break at the radii due to stress concentrations induced by gaps in the toolpath generation. The ASTM D3039 standard was then used for tensile testing (Ahn et al., 2002). Alternately, Lee and Huang (2013) conducted fatigue testing using the ASTM D638

standard and did not report any interference of results when a few samples fractured at the radii.

In Rodriguez et al.'s (2001) research, the ASTM D3039 standard was also used to conduct tensile testing. They concluded a more significant reduction of 22 to 57% in strength relative to ABS monofilament (Rodríguez et al., 2001). This reduction is due in part by voids formed during the process. Default building parameters inherently resulted in voids within generated toolpath previews. Hossain et al. (2013) demonstrated a visual feedback method of adjusting building parameters based on a magnified optical image of the printed part as modifications of parameters using the toolpath preview resulted in gaps that were not identified within the preview.

Toolpaths and other building parameters like build orientation affect the strength of the part inducing an anisotropic nature in FDM created parts. Properties can be considered isotropic within the x-y plane, while strength in the z-direction is measurably less due to the tendency to delaminate between layers (I. Gibson, Goenka, Narasimhan, & Bhat, 2010).

Gibson et al. (2010) investigated a traditional design of living hinge using a PolyJet 3D printing technology that utilizes photopolymer material. Initial results indicated success but encourages further testing for heavy use. Stratasys, Ltd (2013) reports manufacturing an FDM living hinge that lasts up to thousands of cycles. Build recommendations include printing living hinges in a vertical build orientation for the best hinge durability as shown in Figure 3.1. AM living hinges still have room for improvement as traditionally injection molded polypropylene living hinges that can last millions of cycles (Hoffman, 2004).
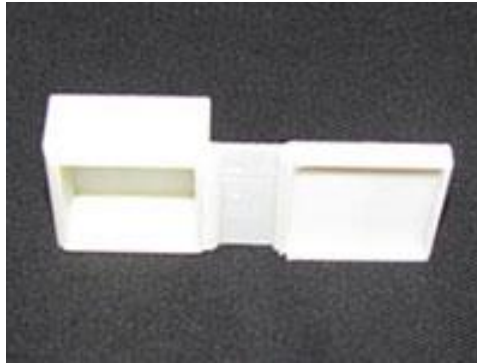
Figure 3.1 FDM living hinge printed in the vertical build orientation (Stratasys, Ltd., 2013)

Experiments

Material Testing

Tensile testing for material properties was conducted to refine the material properties used in the CATIA V5 R20 numerical model. Young's modulus influences how the stress is determined from the deformation/strain on the part. The yield strength sets the failure limit for designing a living hinge to act within the elastic region.

Tensile testing was conducted using the Tinius Olsen Model 290 Lo-Cap Universal Testing Machine with a 133,500 N load capacity. A Tinius Olsen S-400-2A extensometer was used to obtain strain data during tensile testing as shown in the testing setup in Figure 3.2. The strain rate applied was variable with an average of 20 mm/min.

Initial tensile testing was performed to determine proper design geometry between ASTM D3039 (2010) and ASTM D638-10 Type I (2010). The specimen adhering to ASTM D3039 fractured within the grips while the ASTM D638 specimen fractured at the base of the radii similar to the results reported by Ahn et al. (Ahn et al., 2002).
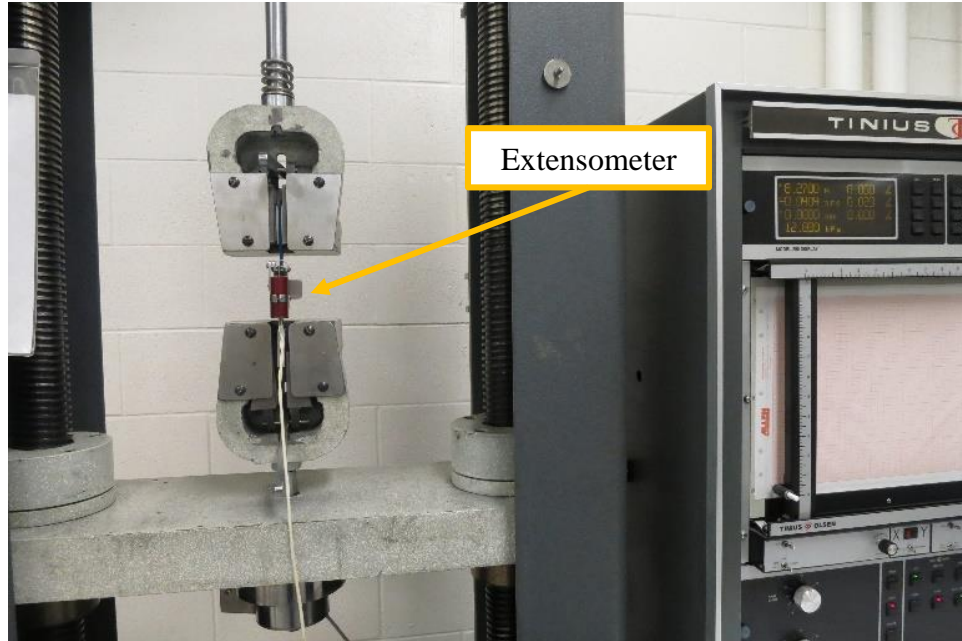
Figure 3.2 Tensile testing setup in the Tinius Olsen with extensometer attached

For the second iteration, 1/8" thick aluminum tabs were applied to the ends of the specimen for better grip and to prevent fracturing within the grips. Another tensile test resulted in the ASTM D3039 specimen fracturing at the location of the tabs. The ASTM D638 specimen again fractured at the base of the radii. Figure 3.3 shows the second iteration specimen failure.
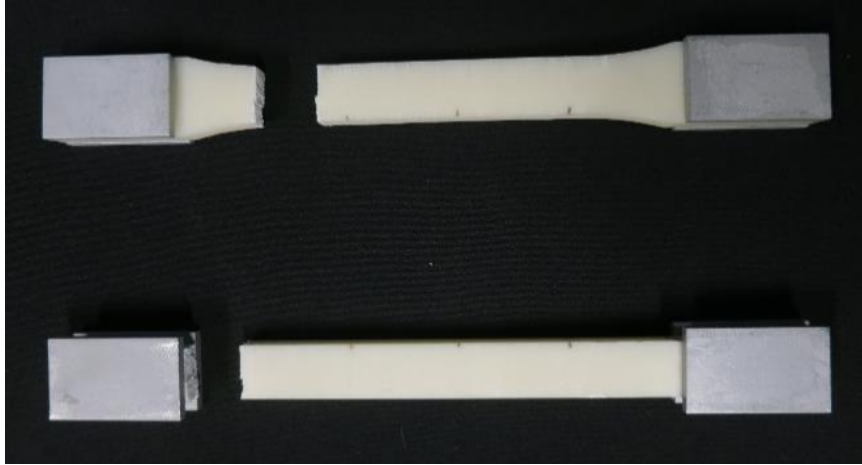
Figure 3.3 Second iteration tensile testing specimen showing ASTM D639 at top fractured at the radii and ASTM D3039 fractured at the tab

The ASTM D638 design geometry was chosen for further testing as it did not fracture within the tab. The crazing displayed along the narrow length of the specimen was more evenly distributed for the ASTM D638 sample, as shown in Figure 3.4a. The crazing in the ASTM D3039 specimen was more concentrated toward the location of fracture as shown in Figure 3.4b.

a)

b)

Figure 3.4 Close-up image of crazing in a) ASTM D638 and b) ASTM D3039

Further refinement of the testing specimen included elongating the ends for more

grip and decreasing the thickness to compensate for the additional thickness provided by

the tabs. The testing area remained the same otherwise. Figure 3.5 displays the quarter

base sketch used to generate the tensile specimen. The overall thickness of the part was

3.5 mm.
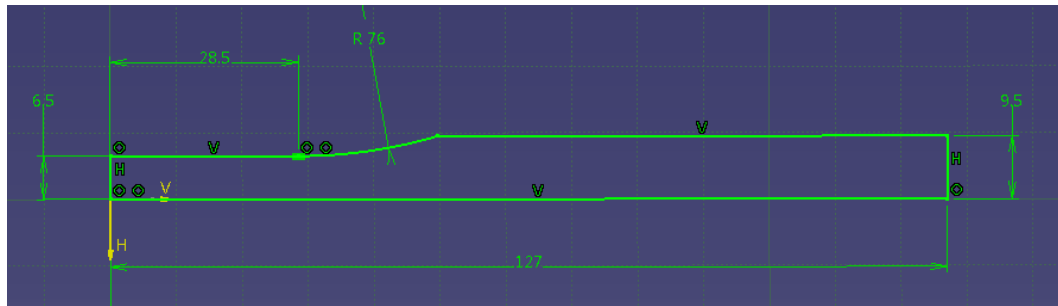
Figure 3.5 CATIA V5 R20 base sketch of one quarter of the tensile specimen (units in mm)

The CATIA V5 R20 part was exported to an STL (stereolithography) file with a

sag size of 0.001 mm and imported into MakerBot Desktop to generate the toolpath data

for printing. The specimen were all arranged to build in the vertical orientation as shown

in Figure 3.6. The specimen were created in the vertical build orientation as the living

hinges were also printed vertically. The same print orientation as the living hinge would

provide material properties that represent the hinge structure.
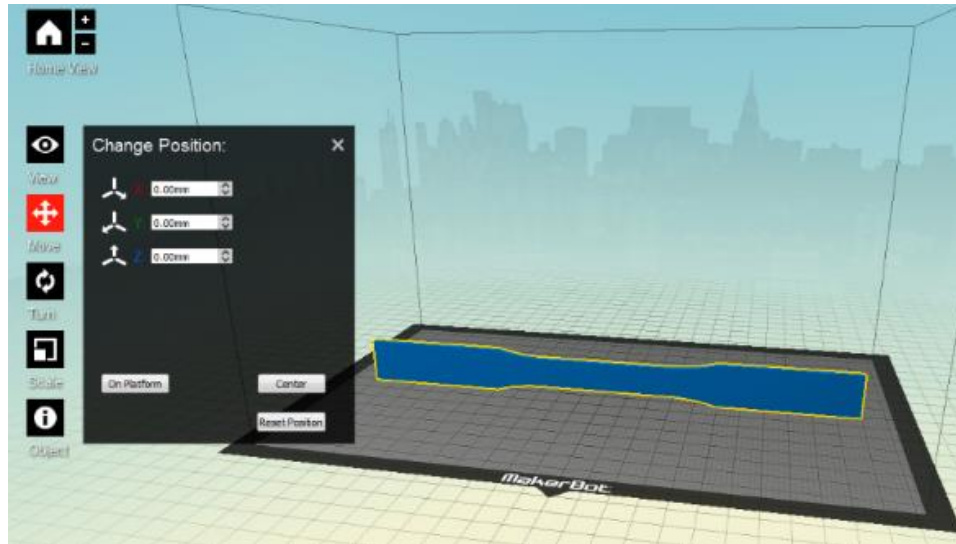
Figure 3.6 MakerBot Desktop Home View position of tensile specimen in vertical print orientation with coordinate system shown under the Change Position box (support structure not shown)

As a result of the vertical orientation, support material was generated to support the part underneath the curve. There is limited control over generation of toolpath direction under the main options so techniques on optimizing building parameters were not utilized. The standard print profile with default values from MakerBot Desktop were used although the infill was changed to 100% for a solid part. Toolpath preview was reviewed and discovered that MakerBot Desktop automatically generates a 45°/-45° alternating toolpath for the outer three layers on a part along the X-Y plane and switches to 0°/90° toolpath for the layers in between. Figure 3.7 illustrates a layer of the tensile specimen that combines the 45°/-45° toolpath for the outer layer of the narrow length of the part and the continuation of the 0°/90° for the left wide tab end. The standard setting also resulted in the presence of voids within the structure as indicated by the print preview.
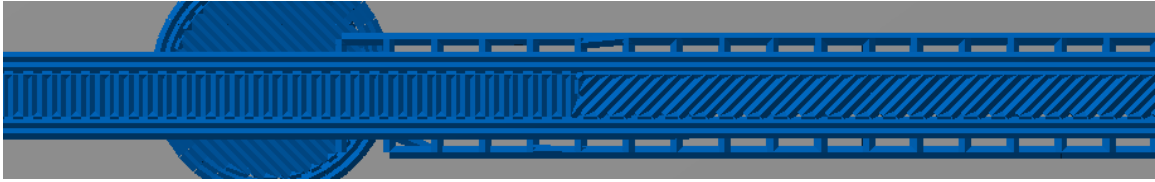
Figure 3.7 MakerBot Desktop top view of the print preview illustrating 0°/90° toolpath on the left and 45°/-45° for the outer layer of the narrow length on the right

The original cross-sectional area to be used in material property calculations was obtained by taking the average of the width and thickness measurements from the narrow section of the tensile specimen. The measurement locations are shown by the black markings in Figure 3.8 using Pittsburg 6" digital calipers with a resolution of 0.01mm.
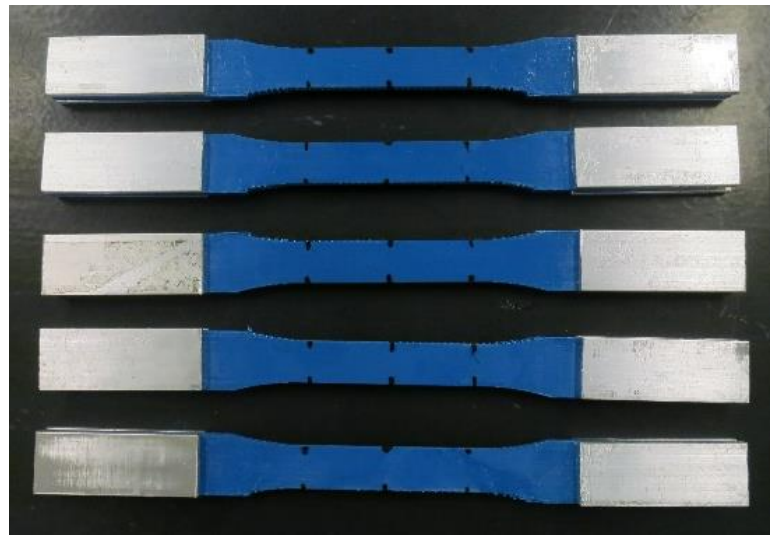
Figure 3.8 Third iteration tensile testing specimen

Application Testing

Experimental testing was planned to be conducted for data on the non-linear, plastic behavior experienced during application, but the micro-tensile machine to be used was unavailable. Fabricating of a living hinge was carried out to determine machine capabilities.

The model containing the traditional living hinge design, as shown in Figure 3.9, was created in CATIA V5 R20. The minimum thickness of 0.3 mm for the hinge thickness would not be rendered by the MakerBot Desktop software in the print preview window when oriented in the vertical print orientation. The hinge thickness was increased by 0.1 mm increments until the MakerBot Desktop software rendered the hinge section in the print preview.
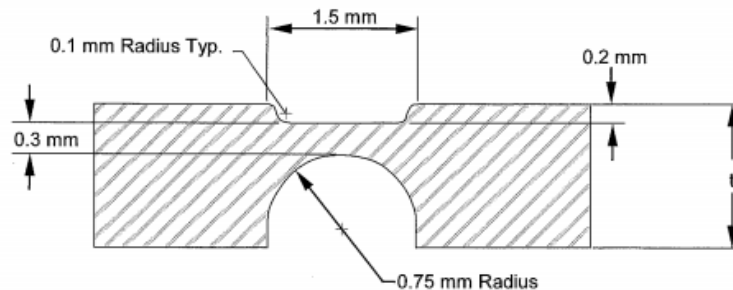
Figure 3.9 Traditional living hinge design (Tres, 2000)

The minimum hinge thickness that MakerBot Desktop would render was 0.6 mm, indicating geometry less than 0.6 mm cannot be printed. The hinge length was also adjusted to 3 mm as demonstrated by the living hinge experimentation by Goenka (2011). The lower recess of the hinge was modified from a semi-circle shape as illustrated in Figure 3.9 to a straight lower fiber with a 0.2 mm radius. The uniform hinge thickness was utilized to follow design suggestions by Stratasys, Ltd (2013). The final design for a printable living hinge on the MakerBot 2X is shown in Figure 3.10.
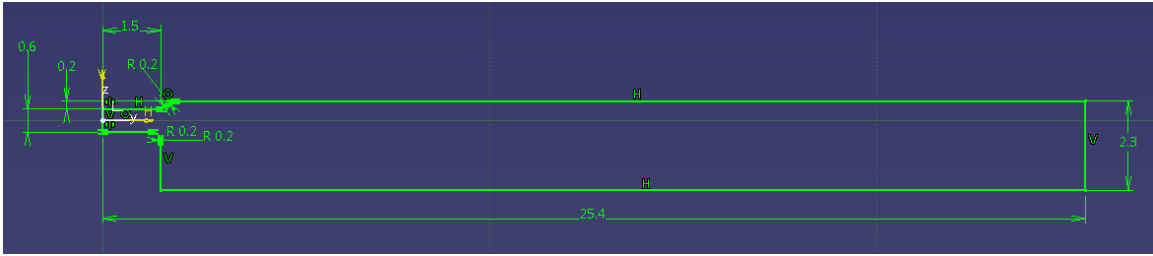
Figure 3.10 CATIA sketch of half a living hinge

The solid model in CATIA was characterized as a material with the Young's modulus and yield strength determined from tensile testing as shown in Figure 3.11. The remaining properties were obtained from CES EduPack (2013). Isotropic material was selected as the anisotropic option contained many necessary properties that were not available.
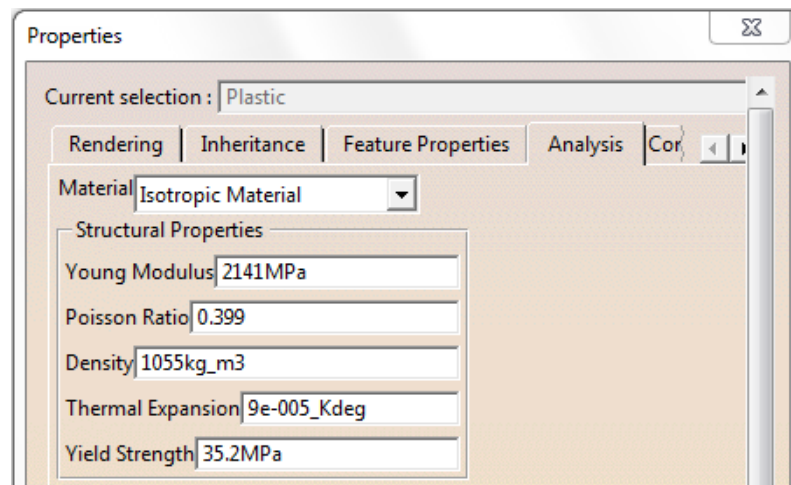
Figure 3.11 Material properties used in the FEA

CATIA's V5 R20 Generative Structural Analysis workbench was used to perform a finite element analysis (FEA) on the solid model. The left face was fully constrained and an enforced displacement was applied on the right end surface as shown in Figure 3.12. A vertical displacement of 4.5 mm was applied for a comparable 10° rotation. The

enforced displacement was defined to use the axis system at the center of the hinge to encourage circular bending
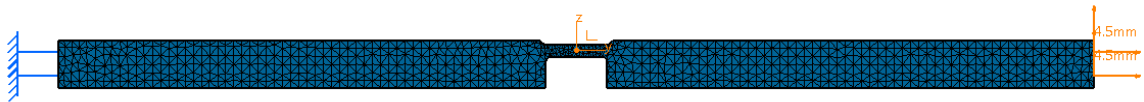
Figure 3.12 FEA case model

An overall part mesh of 0.4mm was generated by CATIA based on the part dimensions. A local mesh size around the hinge area was refined until the resultant maximum von Mises stress was with within 3% of the previous 3 cases. Figure 3.13 displays the local mesh refinement of 0.16 mm about the hinge.
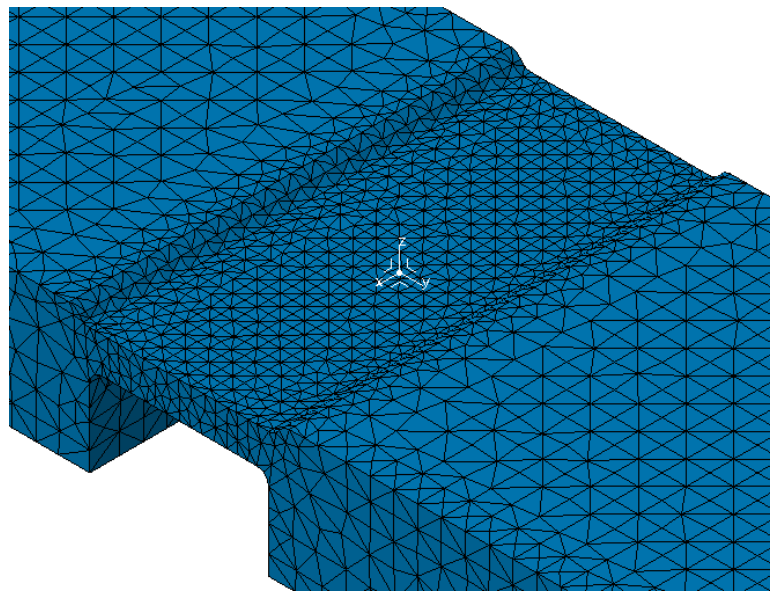
Figure 3.13 FEA local mesh refinement

Furthermore, five living hinge samples were printed and measured for comparison between the theoretical dimensions and the resulting print after shrinkage, which for ABS

is generally about 2% (Pettis, 2013). All hinge specimen were printed in the vertical orientation as recommended by Stratasys, Ltd (2013). The print settings were set to the low/fast setting for MakerBot adjusting only the infill to 100%, the number of shells to 1, and reducing the layer height to the standard setting of 0.2 mm.

Results and Discussion

Material Testing Results

The fracture surface of the ASTM D3039 specimen from the second iteration was examined using a FEI Quanta 650 Scanning Electron Microscope (SEM) under the low vacuum setting. Voids similar to the one shown in Figure 3.14 were discovered. The depth and smooth walls of the void suggests that it was created during manufacturing and not a microvoid from part of the crazing.
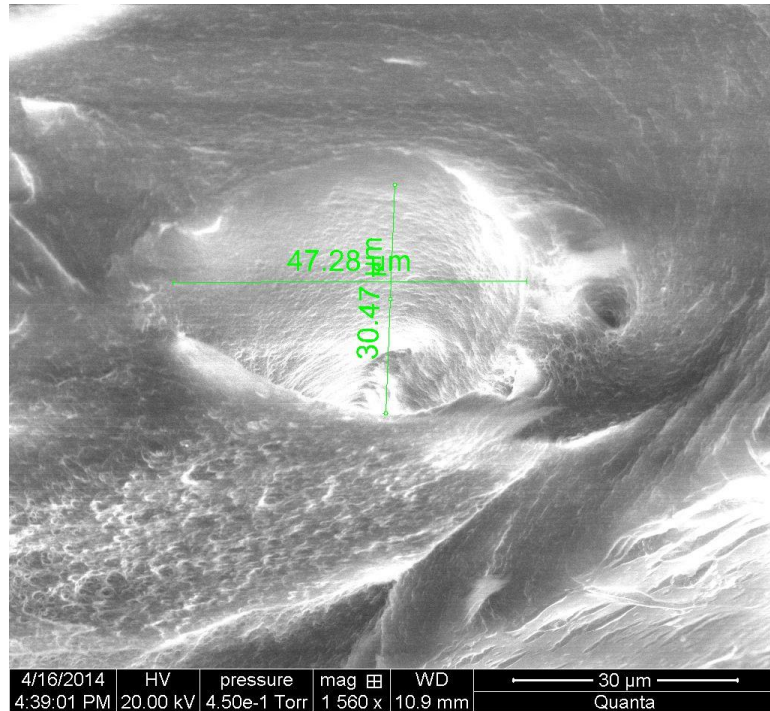
Figure 3.14 Scanning Electron Microscope (SEM) image of tensile testing specimen fracture surface illustrating void measurement of 47.28 μm by 30.47 μm

The measurements for the third iteration of tensile specimen are shown in Table 3.1. The results did not show any pattern on how the values differed at various areas across the narrow section. The thickness was considerably smaller than the theoretical and is attributed to the tendency for ABS to shrink approximately 2%.

Table 3.1 Tensile testing measurements for determination of usable cross-sectional area

Build Orientation	Specimen Number	Width (mm)							Thickness (mm)							Cross-sectional Area, A_0 (mm^2)
		W1	W2	W3	W4	W5	Overall Average (mm)	SD	T1	T2	T3	T4	T5	Overall Average (mm)	SD	
Theoretical		13.00							3.50							45.50
Vertical	I	13.02	12.97	12.96	12.99	12.98	12.98	0.0206	3.36	3.37	3.37	3.36	3.36	3.36	0.0049	43.68
	II	13.16	13.19	13.19	13.17	13.12	13.17	0.0258	3.47	3.49	3.51	3.52	3.52	3.50	0.0194	46.11
	III	13.17	13.15	13.12	13.09	13.18	13.14	0.0331	3.37	3.37	3.36	3.36	3.36	3.36	0.0049	44.21
	IV	13.02	13.06	13.04	12.98	13.00	13.02	0.0283	3.41	3.41	3.41	3.42	3.41	3.41	0.0040	44.42
	V	13.08	13.07	13.08	13.06	13.07	13.07	0.0075	3.41	3.41	3.41	3.41	3.41	3.41	0.0000	44.58
	Sectional Average	13.09	13.09	13.08	13.06	13.07	13.08		3.40	3.41	3.41	3.41	3.41	3.41		44.60
	SD	0.0728	0.0856	0.0861	0.0779	0.0831			0.0434	0.0490	0.0593	0.0654	0.0653			

From the third iteration, all five specimen fractured at the yield strength displaying brittle behavior. The failed specimen are shown in Figure 3.15. As shown, the fracture occurred at the base of the radii but still across an area similar to that measured across the narrow length. A lower strain rate may encourage more plastic behavior.
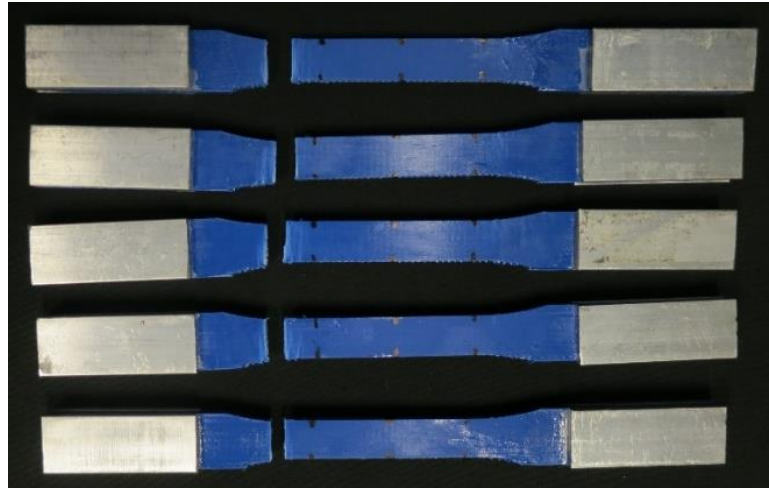
Figure 3.15 Tensile test specimen failure

The engineering stress vs strain curves from the third iteration are displayed in Figure 3.16. The curve displays the same characteristics as Rodriguez et al. (2001) for a test specimen with fibers running perpendicular to the load direction. The fracture toughness of the material may have an influence on the brittle fracture of the specimen if the microvoid is greater than the allowable flaw size. The sample V3 appears to have experienced some slippage in the extensometer near the yield point of the curve, otherwise the results across the five specimen were consistent. The proportional limit of the curves were all around 15 MPa. The Young's modulus was calculated using points at the beginning and end of the modulus line as recommended by an instruction pamphlet from Tinius Olsen (n.d.).
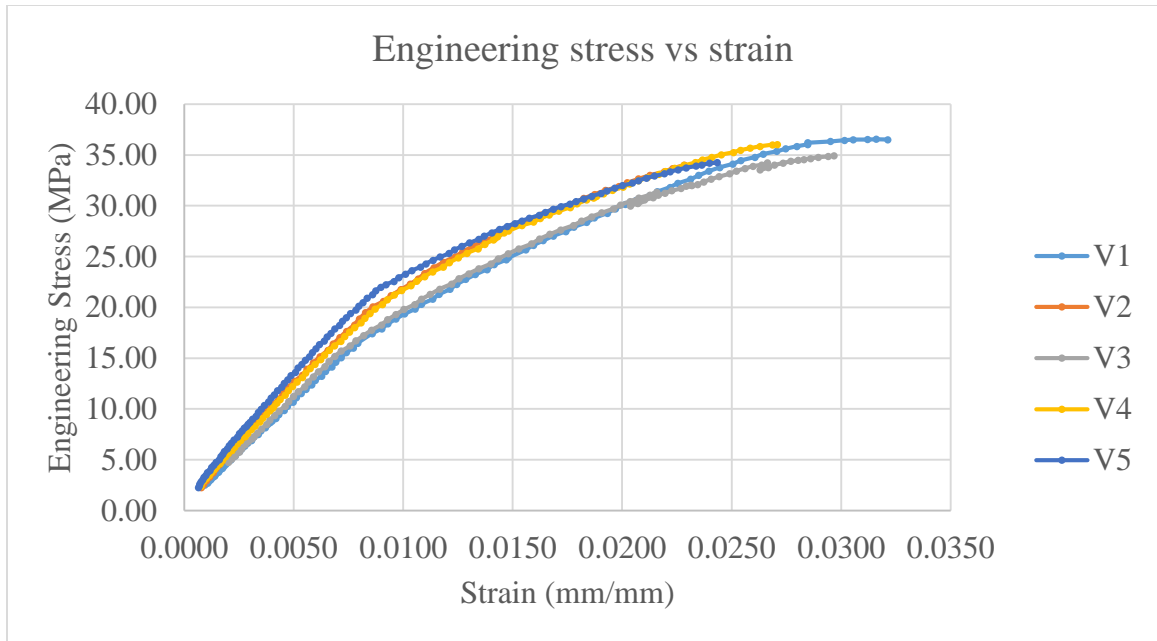
Figure 3.16 Engineering stress vs strain curves from the tensile specimen

The summary of determined material properties for each specimen and the overall average is shown in Table 3.2. The Young's modulus average of 2141 MPa and tensile strength average of 35.16 was used in the adjusted material properties for the CATIA V5 R20 model.

CES EduPack 2013 cites a range of values for each material property and for injection molded ABS the Young's modulus is stated as ranging from 2210 to 2620 MPa. The determined average for FDM ABS of 2141 MPa is 97% of the lower end of the injection molded material. The injection molded range for yield strength is 42 to 46 MPa resulting in the experimental yield strength of 35.2 being 84% of the lower end. The yield strength is a great improvement from previous material studies and can be attributed to the improvement of toolpath generating programs and overlapping fibers.

Table 3.2 Summary of material properties obtained from tensile testing

Specimen	Young's Modulus (MPa)	Yield Strength (MPa)	Yield Strain (mm/mm)
I	1983.59	36.56	0.0321
II	2219.82	34.01	0.0229
III	1985.16	34.93	0.0297
IV	2146.11	36.03	0.0271
V	2370.67	34.27	0.0243
Average	2141.07	35.16	0.0272
SD	147.01	0.99	0.0034

Application Testing Results

From the results of the tensile testing, the failure criteria is defined by stress beyond the yield strength of 35.2 MPa. The translational displacement diagram shown in Figure 3.17 verifies that the hinge deformed as expected about the center of the hinge.
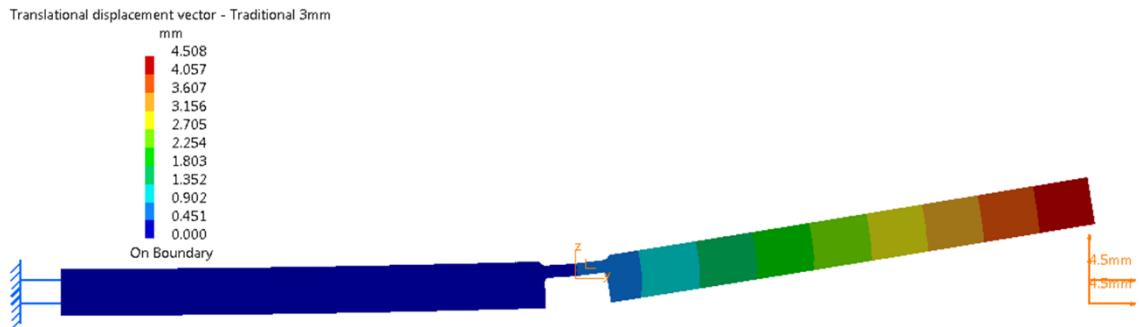
Figure 3.17 Translational displacement vector from CATIA V5 R20 Generative Structural Analysis workbench

Figure 3.18 shows the von Mises stress distribution across the hinge with the yield stress of 35.2 MPa set as the maximum limit. High stress is experienced across the entire hinge with the highest stress experienced is 37.7 MPa under the lower portion of the

61

hinge. This is above the yield stress under a 10° deformation. From the material testing, stress beyond the yield would result in fracture. This current design for a living hinge would not be practical for use with such a minimal operating range.
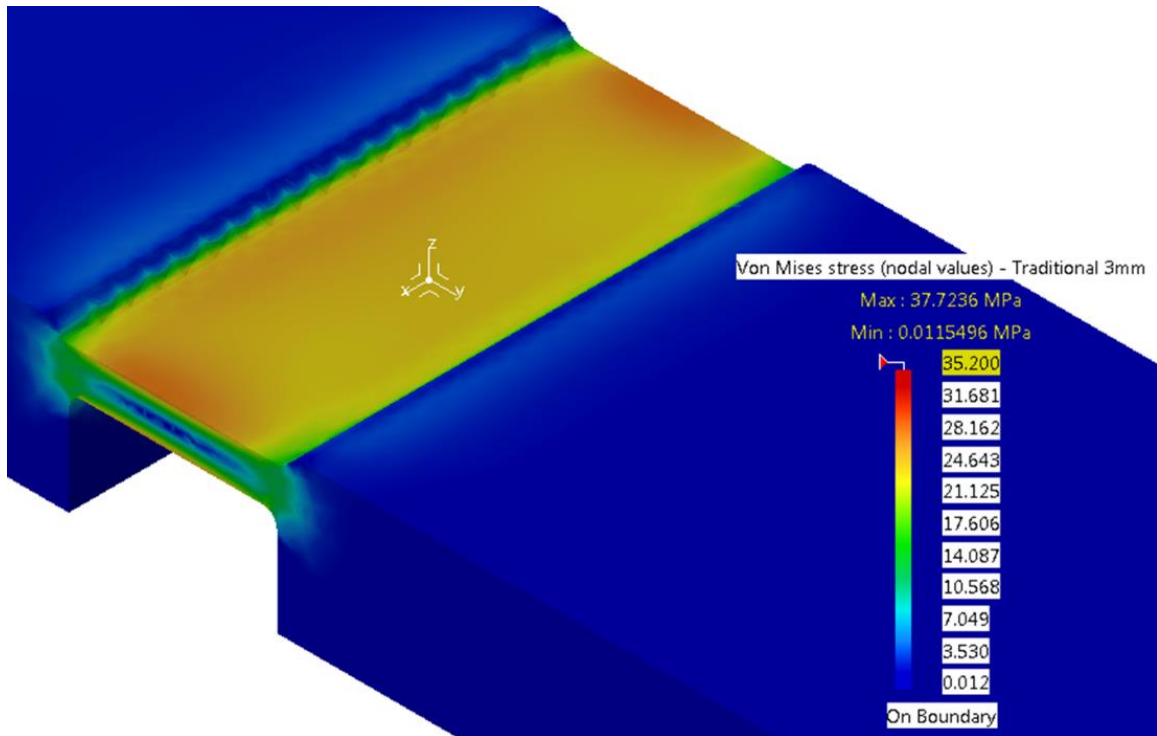
Figure 3.18 von Mises stress distribution from CATIA V5 R20 Generative Structural Analysis workbench

Figure 3.19 displays the printed living hinges with the rearmost hinge placed in the vertical build orientation. It is interesting to note that due to the small design geometry, the lower portion of the hinge resulted in a curve close to the traditional design as shown in Figure 3.9 (introduced on page 54).
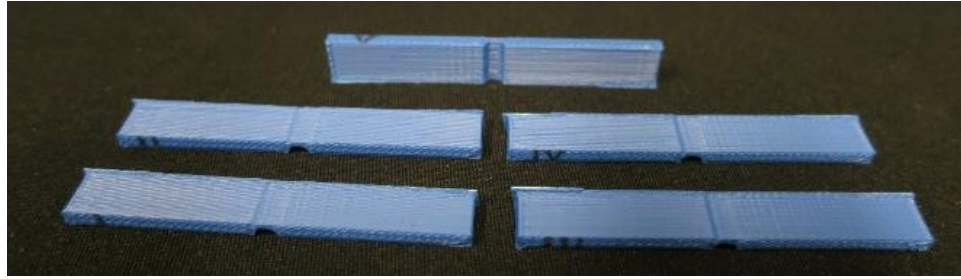
Figure 3.19 Manufactured living hinges with the rearmost hinge shown in the vertical build orientation

The results of the manufactured living hinge sample measurements are shown in Table 3.3. The length and width of the hinge dimensions were all lower than the theoretical while all of the measured thicknesses were all above the theoretical. The same pattern appeared in the overall dimensions with length and width both being lower than theoretical while thickness measured either at or slightly above the theoretical.

Table 3.3 Measurements for a set of traditional designed living hinges

Specimen		Hinge Dimensions			Overall Dimensions		
		Length (mm)	Width (mm)	Thickness (mm)	Length (mm)	Width (mm)	Thickness (mm)
Theoretical		3.00	7.40	0.60	50.80	7.40	2.30
Traditional	I	2.75	7.09	0.94	50.53	7.33	2.31
	II	2.71	7.11	0.93	50.46	7.27	2.30
	III	2.75	7.13	0.94	50.53	7.35	2.31
	IV	2.72	7.11	0.85	50.46	7.27	2.30
	V	2.77	7.12	0.92	50.48	7.25	2.30
	Average	2.74	7.11	0.92	50.49	7.29	2.30
	SD	0.0219	0.0133	0.0338	0.0319	0.0388	0.0049

When taking into account the expectation of ABS shrinking approximately 2%, the overall length and width averages are reasonable measurements while the length and width for the hinge portion are greater than the expected 2% shrinkage minimum. The

effects of small hinge dimensions, as well as its location in the center of the part, may have contributed to a greater than expected shrinkage.

The theoretical value for hinge thickness, while shown to be large enough to manufacture in the print preview, was too small for the printer to create resulting in the apparent minimum thickness that can be printed as approximately 0.9 mm, although printers of similar capabilities can print to smaller values. The overall thickness resulted in nearly theoretical values.

Conclusion and Future Work

Tensile testing showed increased material property values from previously approximated tensile strength, 28.6 MPa to 35.2 MPa. The characteristics of the stress-strain curve displayed brittle behavior that can be attributed to the possibility of microvoids affecting the fracture toughness of the material. Future work into testing and determination of the fracture toughness property for FDM ABS is suggested. As advances in toolpath generation further minimize voids, determining the allowable flaw size is important when designing with respect to the critical stress of the structure.

As recommendations for future work, additional research for improving accuracy of small structures like living hinges using a MakerBot 2X would involve exploring the advanced options of MakerBot Desktop. Adjustment of the advanced options requires understanding of MakerBot terminology of the different parameters and how they affect the overall build.

Alternate designs for living hinges would be a study of interest for further research. The traditional design for a living hinge allows too high of a stress

concentration in the small area as indicated by the FEA. Suggestions include elongating

the hinge length or experimenting with completely new design geometries like zigzag or

wave patterns.

References

Ahn, S.-H., Montero, M., Odell, D., Roundy, S., & Wright, P. K. (2002). Anisotropic material properties of fused deposition modeling ABS. *Rapid Prototyping Journal*, *8*(4), 248–257.

ASTM Committee D-20 on Plastics., A. S. D. 1. on M. P. (2010). *Standard test method for tensile properties of plastics.* Philadelphia, Pa.: ASTM International.

ASTM International. (2010). *Standard test method for tensile properties of polymer matrix composite materials.* West Conshohocken, Pa.: ASTM International.

CES EduPack 2013. (2013). ABS (injection molding, platable). Granta Design Limited.

Gibson, I., Goenka, G., Narasimhan, R., & Bhat, N. (2010). Design Rules for Additive Manufacture. In *International Solid Freeform Fabrication Symposium An Additive Manufacturing Conference* (Vol. 2010, pp. 705–716). Austin, Texas: The University of Texas at Austin.

Gibson, I., Rosen, D. W., & Stucker, B. (2010). *Additive manufacturing technologies rapid prototyping to direct digital manufacturing*. New York; London: Springer. Retrieved from http://dx.doi.org/10.1007/978-1-4419-1120-9

Goenka, G. (2011). *Modeling and investigation of elastomeric properties in materials for additive manufacturing of mechanistic parts*. National University of Singapore, Singapore.

Hoffman, J. M. (2004, August 19). Care and feeding of living hinges. *Machine Design*, *76*(16), 64, 66.

Hossain, M. S., Ramos, J., Espalin, D., Perez, M., & Wicker, R. (2013). Improving Tensile Mechanical Properties of FDM-Manufactured Specimens via Modifying Build Parameters. In *International Solid Freeform Fabrication Symposium An Additive Manufacturing Conference* (Vol. 2013, pp. 380–392). Austin, Texas: The University of Texas at Austin.

Interpretation of Stress-Strain Curves and Mechanical Properties of Materials. (n.d.). Tinius Olsen Testing Machine Co., Inc. Retrieved from http://www.tiniusolsen.com/pdf/Pamphlet4.pdf

Lee, J., & Huang, A. (2013). Fatigue analysis of FDM materials. *Rapid Prototyping Journal*, *19*(4), 291–299. doi:10.1108/13552541311323290

Pettis, B., France, Anna Kaziunas., Shergill, Jay.,. (2013). *Getting started with MakerBot*. Sebastopol, Calif.: O'Reilly.

Rodríguez, J. F., Thomas, J. P., & Renaud, J. E. (2001). Mechanical behavior of acrylonitrile butadiene styrene (ABS) fused deposition materials. Experimental investigation. *Rapid Prototyping Journal*, *7*(3), 148–158. doi:10.1108/13552540110395547

Stratasys, Ltd. (2013). Functional Prototyping - Living Hinges. Retrieved from http://www.stratasys.com/applications/functional-prototyping/living-hinges

Tres, P. A. (2000). *Designing Plastic Parts for Assembly* (4th ed.). Cincinnati: Hanser-Gardner.

Chapter 4

Exploration of Alternate Living Hinge Designs for Entry Level FDM Systems

Cassandra S. Gribbins

Embry-Riddle Aeronautical University

This article would be submitted to the Rapid Prototyping Journal for the special issue Entry Level Additive Manufacturing: The Next Frontier and would summarize the analysis and fabrication of alternate living hinge designs.

"This freedom of design is one of the most important features of RM and is extremely significant for producing parts of complex or customized geometries, which will result in reducing the lead-time and ultimately the overall manufacturing costs for such items" (Hopkinson, Hague, & Dickens, 2006, p. 6).

Abstract

The aim of this research is to explore alternate geometric designs for living hinges to more evenly distribute stress across the hinge compared to a traditional design. The alternate designs include elongated traditional hinge designs, a zigzag design, a lamella design, and a wave design. Alternate hinge designs were created based on minimum printing capabilities of a MakerBot 2X. The solid models of the hinges were analyzed by finite element analysis to observe stress distribution and obtain a maximum experienced von Mises stress to compare with the material's yield stress of 35.2 MPa. An elongated hinge design allowed for more area for the stress to distribute. The wave design was the optimal of the designs experiencing a maximum von Mises stress of 10.3 MPa. Further experimental research on the accuracy of the FEA results is planned for validation. Optimization of the alternate hinge design geometries can be explored with respect to the capabilities of different fused deposition modeling machines. The research provides a starting point for implementing living hinges in designs that utilize the geometric freedom provided by additive manufacturing. Living hinges themselves offer the benefit including consolidating the number of parts in assembly. This paper adds knowledge to the limited data on living hinges manufactured through entry-level fused deposition modeling machines. Previous studies exploring alternate hinge designs have focused on utilizing expensive selective laser sintering technologies.

69

Introduction

Living hinges are a common design feature used in plastics that incorporate bending in a single piece without the need of additional joining parts or assemblies. This is accomplished by having the two thicker walls connected by a relatively thin portion of material (Tres, 2000).

A traditional living hinge design is characterized by a recess on the top potion of the hinge and the complete arc at the bottom as shown in Figure 4.1a in the open position. The arc at the top guides the bending of the material to help prevent cracking while the arc in the lower portion encourages proper flexing as shown with the hinge in the closed form in Figure 4.1b.

In the automobile industry, living hinges have been used in electrical junction box covers as shown in Figure 4.2 (Kim, Son, & Im, 2003). The hinges act as built-in fasteners with a snap-fittings reducing the need for additional parts.
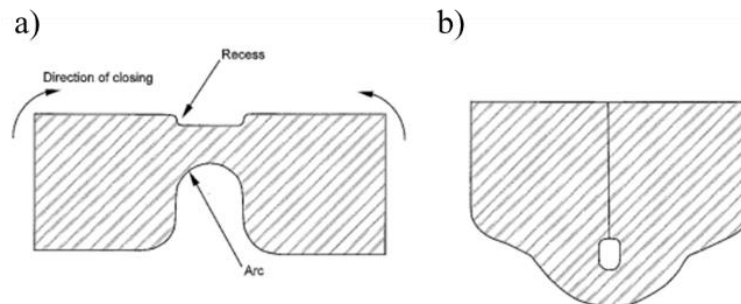
Figure 4.1 Traditional living hinge geometry (Tres, 2000)

Reducing part count is an important aspect for the Design for Assembly (DFA) methodology which include guidelines for product development (Poli, 2001). Design for Manufacturing (DFM) is a methodology that also provides guidelines for developing part

designs but with specific consideration to the capabilities of manufacturing processes

(Poli, 2001). For injection molding, an ideal part is ejected with as little tooling

complexity as possible. Complex geometry containing features like undercuts could

necessitate expensive moving parts within the die (Hague, Mansour, & Saleh, 2004).

Figure 4.2 Two sets of living hinges on an automobile electrical junction box cover (Kim et al., 2003)

Design guidelines suggesting minimizing part complexity do not impact additive

manufacturing (AM) as greatly as other traditional manufacturing processes. With this

lifted restraint of design complexity, reduction of part count by consolidating parts is

more easily executable (Hague et al., 2004; Hopkinson et al., 2006). An example of the

impact AM has on DFM and DFA is shown in Figure 4.4 with an aircraft ducting

assembly being consolidated to a single piece.
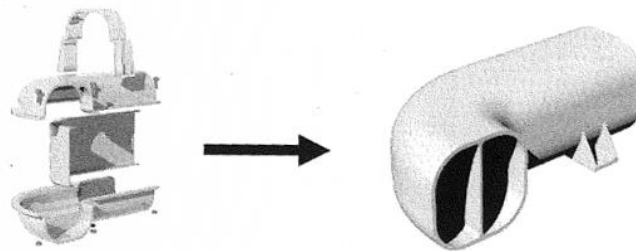
Figure 4.3 Aircraft ducting example of part consolidation

Previous research indicated that the traditional living hinge design experienced stress close to the yield strength under a 10° deformation (Gribbins & Steinhauer, 2014). Figure 4.4 shows the traditional hinge design Gribbins and Steinhauer referenced as a basis for a printable hinge. The traditional design had to increase the thickness to 0.6 mm and increase the length to 3 mm to fit the minimum resolution of the MakerBot 2X used. The CAD model of the hinge was deformed 10° and observed to be experiencing stresses beyond the allowable yield stress. To resolve this, changing the geometry was encouraged.
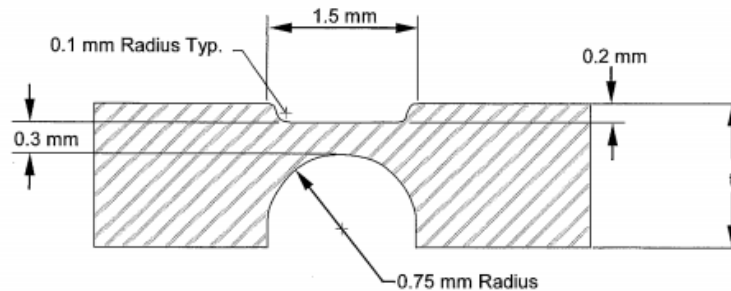
Figure 4.4 Traditional hinge design geometry (Tres, 2000)

A Stratasys design blog (Stratasys, Ltd., 2013) encourages elongating living hinge length for better durability as well as printing the hinge vertically. The vertical orientation follows general FDM design guidelines that suggest building parts in an orientation in which the tensile loads would be axially carried along the fibers (Ahn, Montero, Odell, Roundy, & Wright, 2002). This manufacturing consideration differs from the guideline for creating hinges via injection molding in which the polymer must flow across the hinge length to prevent premature hinge failure (Hoffman, 2004).

Gonzalez and Kerl (2008) from the AM machine manufacturer, EOS, performed a design study on alternate living hinge designs for the laser sintering process. General

design suggestions were to keep the hinge small in size with an emphasis to have a very thin thickness. The objectives of the alternate hinge designs was to achieve smooth bending. During application, living hinges experience fatigue, tensile compression, and sometime dynamic stresses (Elleithy, 2007). The zigzag design shown in Figure 4.5a was described positively as having simple geometry and the ability to bend 360°. Figure 4.5b shows the wave design that demonstrated no stress peaks. The lamella design shown in Figure 4.5c demonstrated equal movement in both directions. The zigzag and wave structures were built vertically while the lamella was built horizontally.
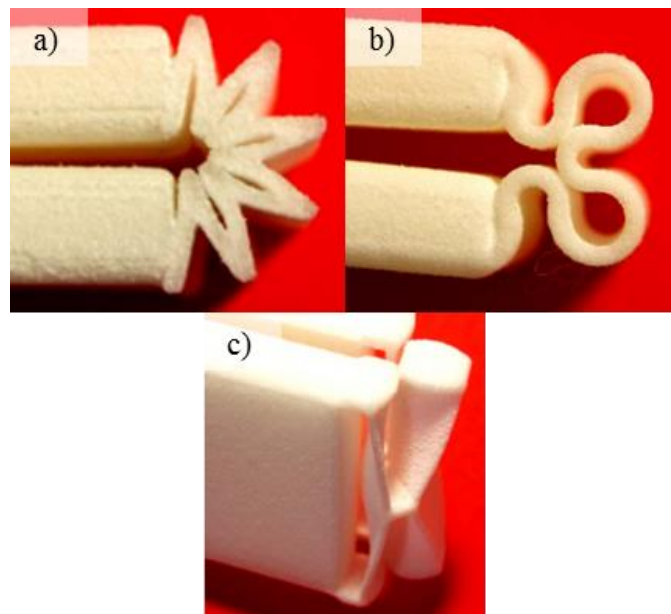
Figure 4.5 EOS alternate living hinge designs: a) zigzag, b) wave, and c) lamella (Gonzalez & Kerl, 2008)

The 3D printing marketplace for designers and consumers, Shapeways, describes two strategies for modeling living hinges for their "white strong and flexible" plastic material. One is a 'harmonica' structure shown in Figure 4.7a. This design is similar to

the zigzag design referenced in the EOS research. The thickness of each line is recommended to be 0.5mm.

The Shapeways design blog also describes utilizing an unnamed design that is similar to EOS' lamella. The structure, shown in Figure 4.7b, also recommends a thin wall thickness of 0.5 mm.
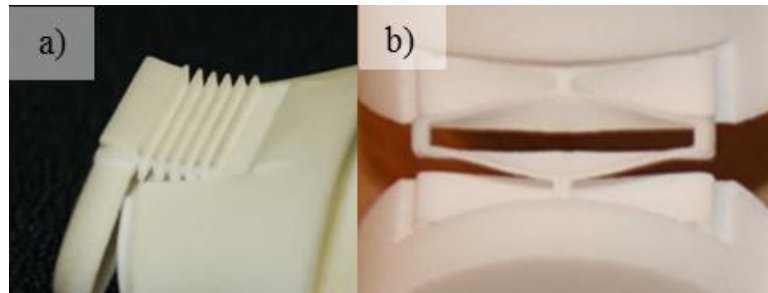
Figure 4.6 Shapeways alternate living hinge designs: a) harmonica and b) unnamed (bart, 2008)

Experimental Setup

Alternate designs explored in this study consisted of two elongated traditional designs, a zigzag design, lamella structure, and wave design. CATIA V5 R20 was used to design and analyze stress distribution within the hinges.

The two variations of the traditional hinge kept the same radii and thickness measurements. Although inaccuracy with printing the small thickness of 0.6 mm have been documented, the thickness was kept the same to observe if print accuracy is affected by the geometric design of the part (Gribbins & Steinhauer, 2014). The hinge length was increased to 6 mm and then 12 mm. Figure 4.7a displays the base sketch for the 6 mm traditional type and Figure 4.7b shows the 12 mm version.

74
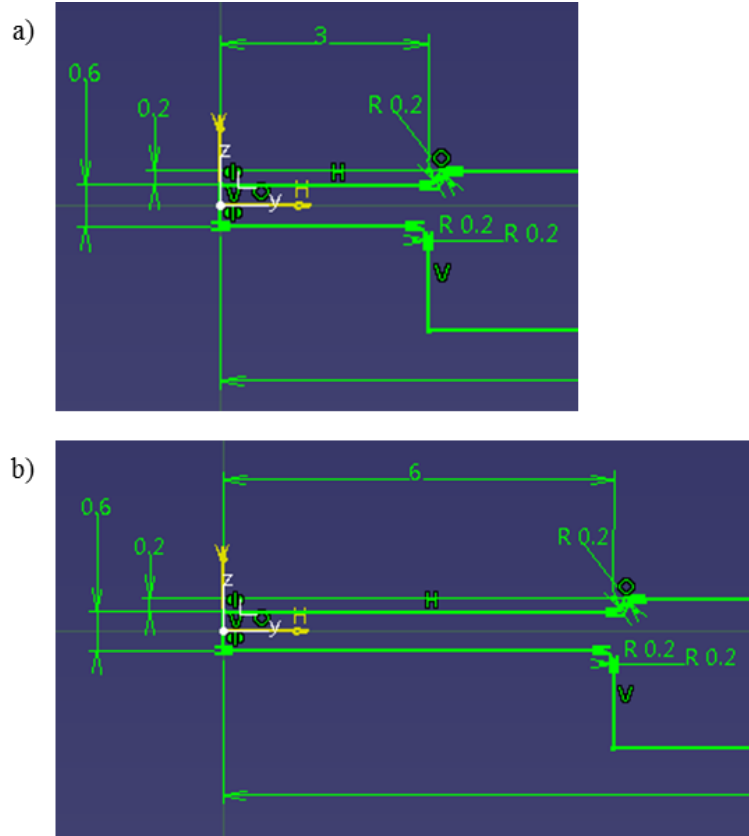
Figure 4.7 Traditional a) 6 mm and b) 12 mm type base sketches

Dimensions for the alternate designs were established using the traditional 12 mm

design as a base sketch for optimal space to employ the complex geometries. The

alternate designs were further constricted to a design envelope of a height of 2.3 mm, 3.7

mm width based on the values established in the previous study to allow for comparison

of results. Geometrical constants such as tangency were also utilized to fully constrain the

model.

Figure 4.8 shows the base sketch for the zigzag design based off of the EOS

design in Figure 4.5a. An additional peak was added to maintain symmetry across the

part. The peaks were also constrained to the top and bottom surfaces of the hinge,

utilizing the full design envelope. A constant fiber thickness of 0.6 mm was also applied.
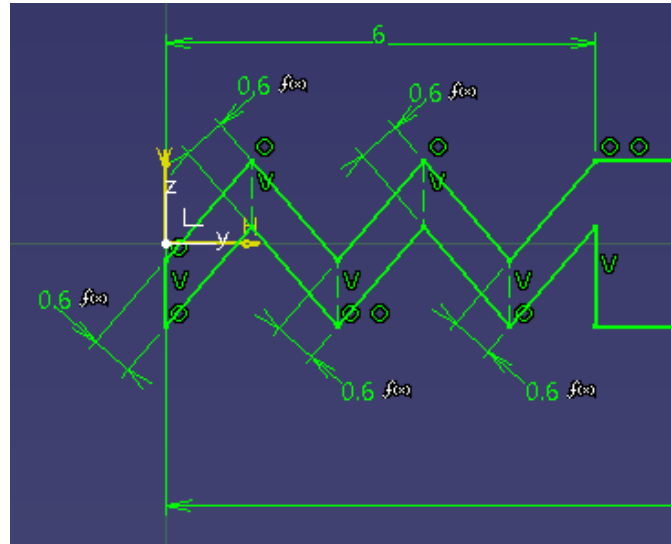
Figure 4.8 Zigzag type base sketch

The base of the lamella structure was the same as the traditional 12 mm sketch as

shown in Figure 4.7b. The pockets of the lamella were geometrically constrained to the

edges of the hinge to maximize use of the build envelope. Keeping the initial width of the

fibers to 0.6 mm conflicted with MakerBot Desktop and displayed missing and floating

segments during print preview. The width of the fibers were then increased by 0.1 mm

until the complete structure displayed in the MakerBot Desktop print preview. This

process resulted in a usable fiber width of 1.2 mm as shown in Figure 4.9.
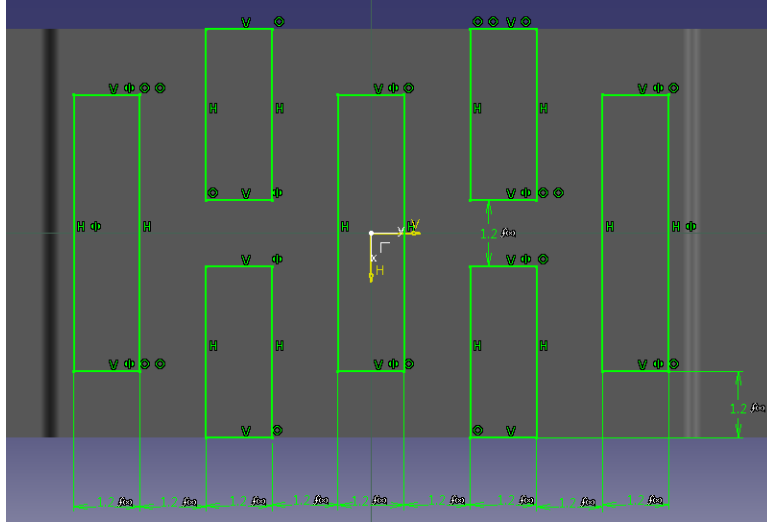
Figure 4.9 Lamella type top pocket sketch

The wave type design was defined by the center radius constrained to the overall part center to encourage appropriate circular bending of the hinge. The value of the radius was established as half of the overall height of 2.3 mm. Tangency constraints further defined the fully constrained design of the wave type as shown in Figure 4.10.
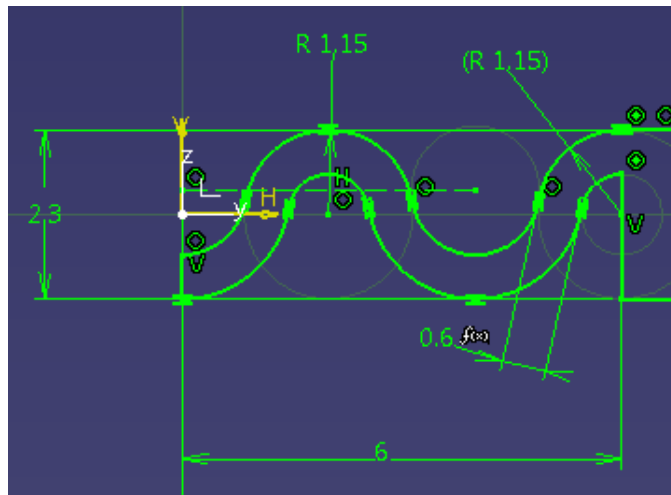
Figure 4.10 Wave type base sketch

The hinges were printed in acrylonitrile butadiene styrene (ABS) on a MakerBot 2X under the low/fast setting adjusting only the infill to 100%, the number of shells to 1, and reducing the layer height to the standard setting of 0.2 mm. All hinges were printed vertically as the horizontal orientation suggested by EOS introduced too much support structures that would not be easily removed without affecting the integrity of the geometry.

The finite element analyses (FEA) of the hinges was executed using the Generative Structure Analysis workbench in CATIA V5 R20. Material properties of FDM ABS from the previous tensile testing research were applied to the solid model. Figure 4.11a shows the case model with the fixed constraint and enforced displacement.

A static analysis case was chosen with a parabolic element type rather than linear type for a more accurate solution (Zamani, 2010). The options for the OCTREE Tetrahedron Mesh were left as the default to start as the program adjusts the size with respect to the solid model. After running a case, a localized mesh around just the hinge was refined until the resultant maximum von Mises stress values varied less than three percent between cases. Figure 4.11b shows the refined mesh.

A fixed constraint and enforced displacement were established as the boundary conditions for the case. The fixed constraint was applied to the leftmost surface to restrict movement of all translation and rotation on that surface.
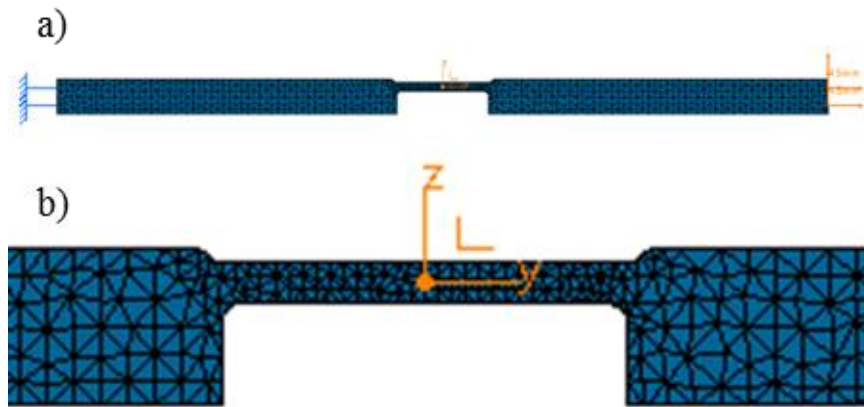
Figure 4.11 FEA hinge model: a) side view with fixed end on the left and enforced displacement on the right and b) close up of refined mesh with referenced coordinate system located in the center

A 10° rotation on the rightmost face was desired for the enforced displacement, but due to complications in applying a rotation command for a 3D model, a comparable vertical translation of 4.5 mm based on the half length of the solid model was applied. The horizontal component, which would induce approximately 1.5% strain, was not included in the analysis. The enforced displacement referenced a coordinate system in the center of the hinge to encourage circular bending about the hinge.

Results and Discussion

The manufactured living hinges are shown in Figure 4.12. Figure 4.12a and b display the 6 mm and 12 mm hinge lengths for the traditional design. Printing was straightforward with limited difficulties aside from an issue of lifting at the ends of the part that commonly occurs in long, thin parts. The lifting is due to the force generated by the material shrinking and pulling the cooler extremities to the hotter center. Small, circular, two layer thick rafts obtained from Thingiverse (2012) were intersected with the

ends to add more surface area and keep the ends attached to the build plate without resorting to altering the center hinge geometry. The rafts were easily removed with an X-Acto knife. The zigzag and wave designs shown in Figure 4.12c and e had similar lifting issues and were resolved with the addition of rafts.

The center geometry of the lamella design in Figure 4.12d consisted of layers in the beginning of the print that were too small and would not stay attached to the build plate. The lamella is the only hinge design that needed additional rafts in the center to keep the part on the build plate. Great care was taken to cut away the rafts after manufacturing without prematurely bending or introducing stress to the hinge. The lengthy post-processing is a disadvantage to the design.
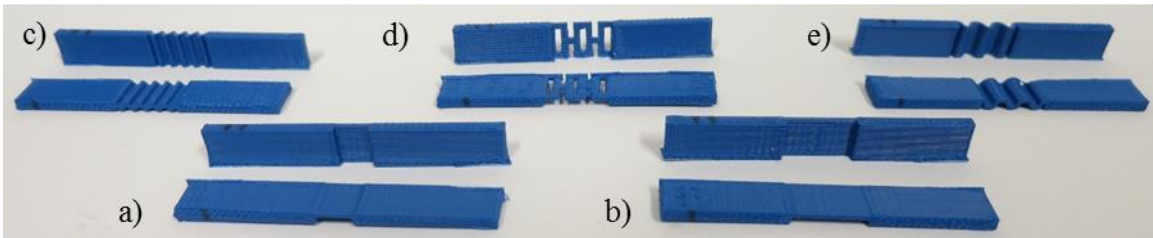
Figure 4.12 Printed living hinges: a) Traditional 6 mm, b) Traditional 12mm, c) Zigzag, d) Lamella, and e) Wave

The average length measurement of 5.82 mm for the traditional 6 mm was beyond the acceptable 2% shrinkage limit of 5.88 mm from the theoretical value. The traditional 12 mm, zigzag, and lamella designs also measured less than the shrinkage limit as shown in Figure 4.13. Only the wave design fell within the allowable values. The greater shrinkage of the hinge length is understandable as the center of the part would be more affected by the force of the shrinking material. The wave design was closer to the

theoretical because there was more surface area on the build plate to hold geometry in place.
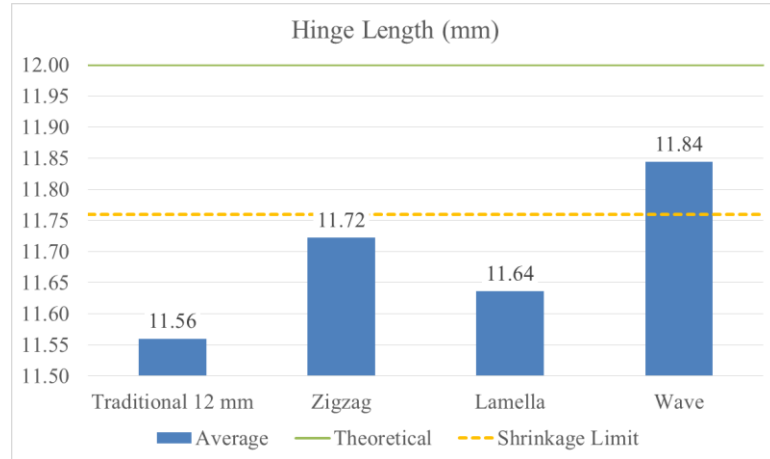
Figure 13 Hinge length averages compared to theoretical and shrinkage limit values

Figure 14 shows the hinge width averages. The measurements from the traditional designs were beyond the shrinkage limit of 7.25 mm. The zigzag design was close to the limit while the lamella and wave designs had acceptable measurements. The complex geometry of the alternate designs contributed to the prevention of the part from shrinking too much.
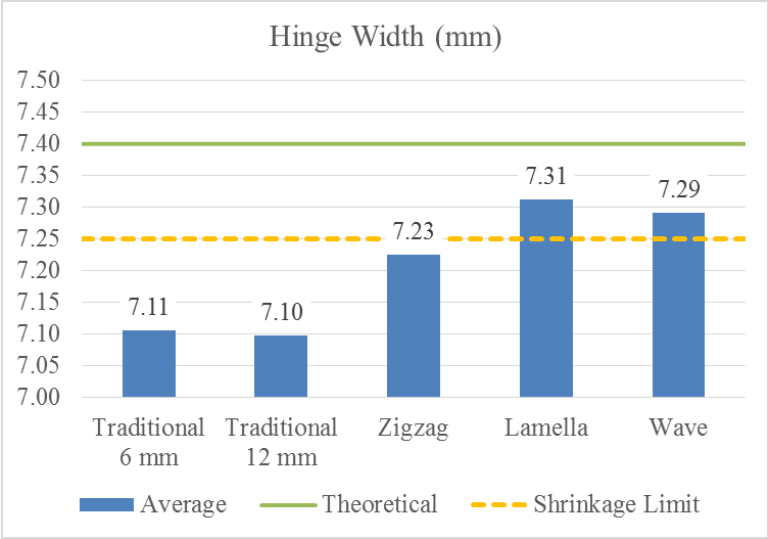
Figure 4.14 Hinge width averages compared to theoretical and shrinkage limit values

The hinge thickness measurements were all greater than the theoretical 0.6 mm as shown in Figure 4.15. The greater thickness values infer that the theoretical thickness is too small for the capabilities of the printer. A smaller layer thickness may result in a value closer to the theoretical.
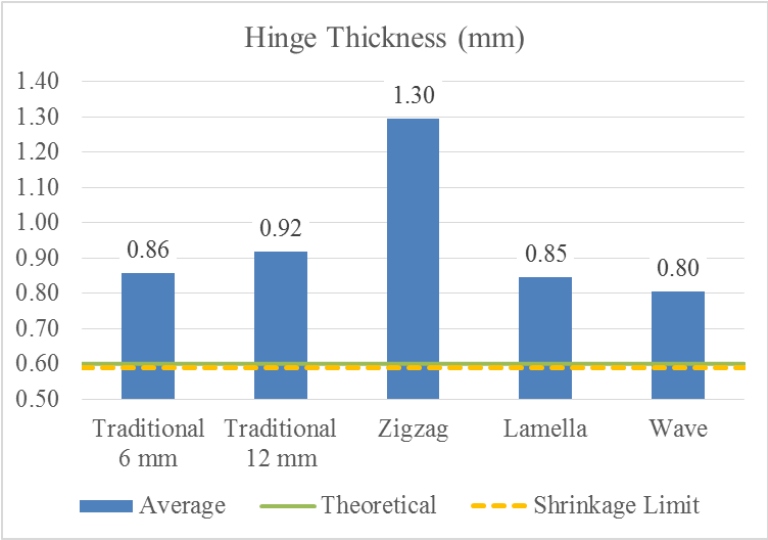
Figure 4.15 Hinge thickness averages compared to theoretical and shrinkage limit values

Figure 4.17 shows the stress distribution of the traditional 6 mm type with a maximum stress of 21.5 MPa. Though displacement was referenced to the center of the hinge, the concentration is slightly shifted to the area closest to the fixed end suggesting that rotation is occurring at the connection between the hinge and thicker tab.
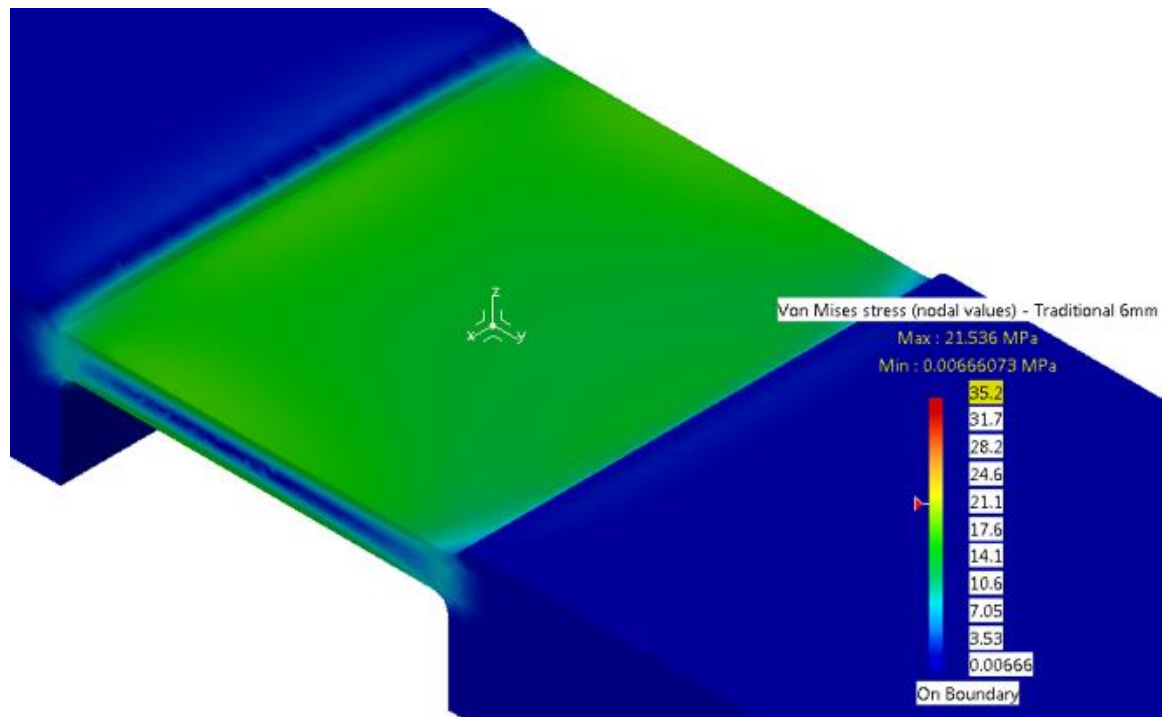
Figure 4.16 Traditional 6mm type von Mises stress distribution

The stress distribution for the traditional 12 mm design is shown in Figure 4.18 with a maximum stress of 14.1 MPa which is less than the 6 mm version and shows that increasing the length encourages the stress to further distribute over the hinge. Again, the focus of the stress is more concentrated towards the fixed end of the hinge and the nearby edges indicating that rotation is occurring at the end of the hinge connection rather than the center of the hinge.
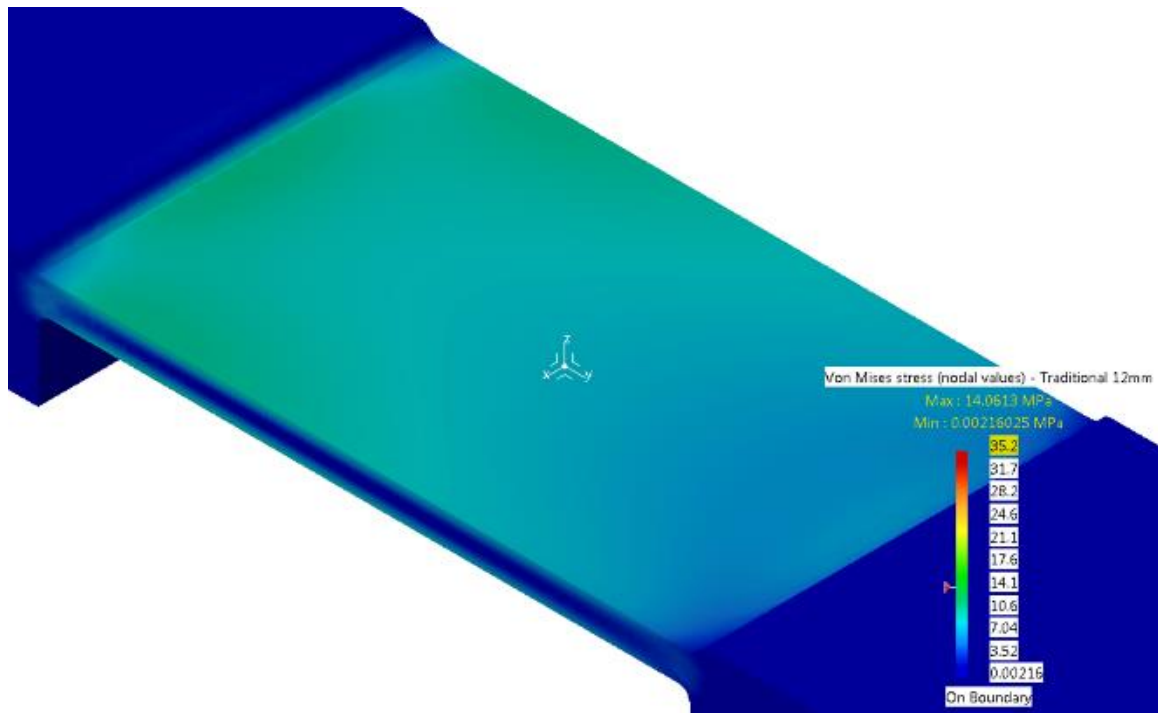
Figure 4.17 Traditional 12mm type von Mises stress distribution

The zigzag alternate design experienced a maximum stress of 12.3 MPa within the inner crease of the peaks toward the fixed end of the part shown in Figure 4.19. The stress variation between the inner segments were relatively small which indicates that rotation was distributed between the segments rather than concentrating in a single area like the traditional hinge design. The peaks experienced little to no stress suggesting that the geometry there is unused and can be rounded off in future designs.
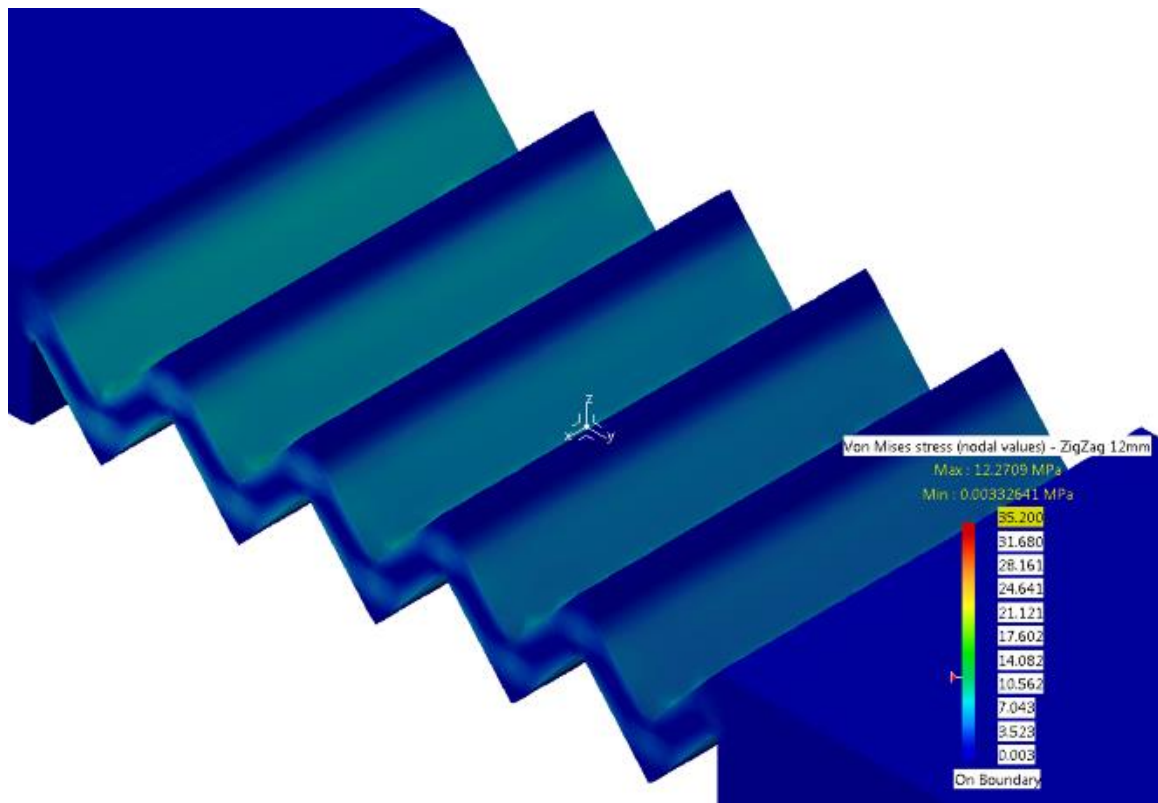
Figure 4.18 Zigzag type von Mises stress distribution

The lamella type experienced stress concentrations at the inner corners as shown in Figure 4.20 producing a maximum von Mises stress of 18.9 MPa. Based on the manufactured hinge from Figure 4.12d, the inner corners are slightly rounded due to shape of the fibers. Sharp geometries were not expected as the printer cannot achieve sharp details due to the nature of the process. The rounded geometry suggests that the high stress concentration indicated by the FEA may be excessive. On the other hand, it is not known how much the layered composition has weakened the small area. An experimental analysis is needed to determine the extent of the stress on the overall hinge. The outer corners of the design show little to no stress suggesting that the material there is not needed and therefore could be replaced with rounded off corners. Increasing the number of connections between segments would further distribute the stresses.
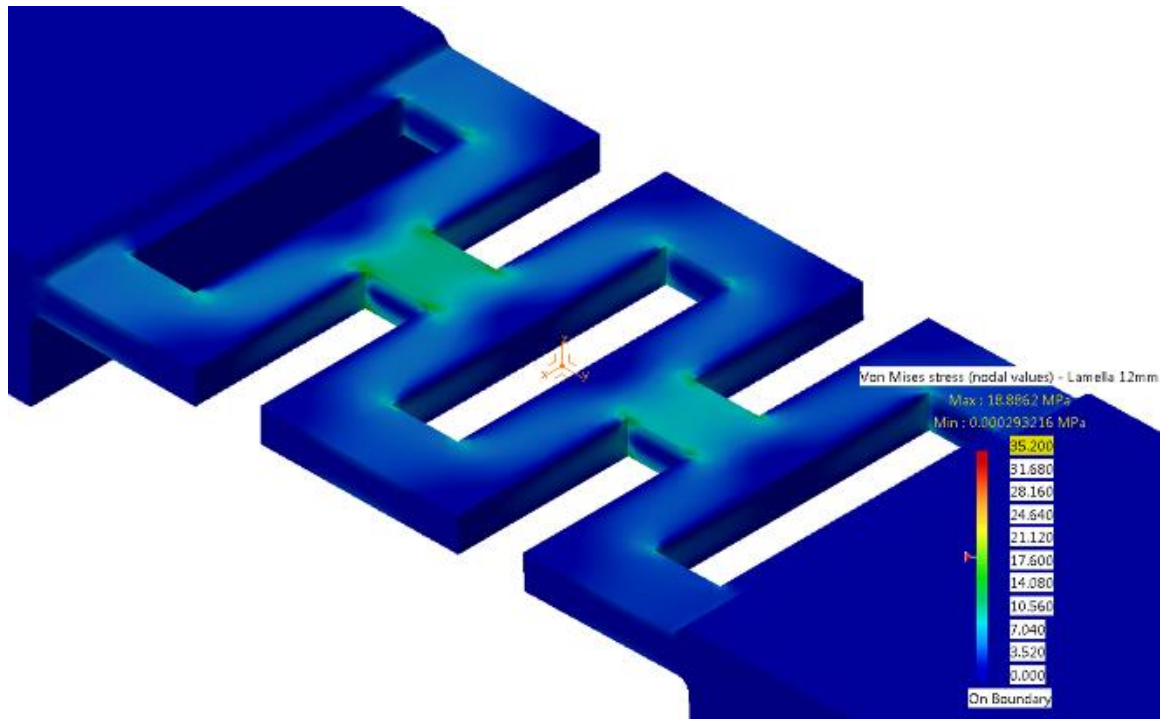
Figure 4.19 Lamella type von Mises stress distribution

The wave type living hinge variant resulted in the lowest maximum von Mises
stress of the designs analyzed experiencing 10.3 MPa. Again, the focus of stress was on
the portion of the part toward the fixed end as shown in Figure 4.21. Similar to the zigzag
design, the difference of stresses between the high stressed inner radius and the others are
relatively small which also indicates that rotation was balanced between the segments
rather resulting in a more even stress distribution. The neutral axis experienced little to no
stress across the entire hinge further indicating elastic behavior within the hinge.
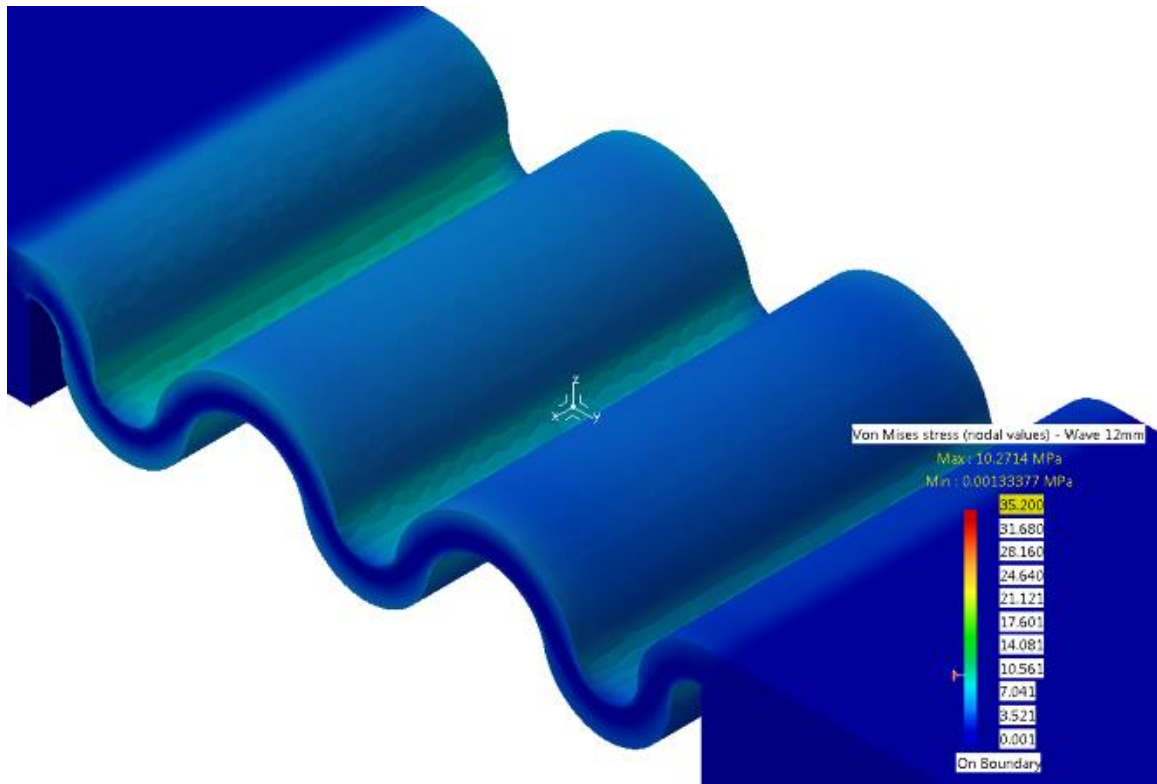
Figure 4.21 Wave type von Mises stress distribution

The summary of results from the CATIA V5 R20 FEA analysis is shown in Table 4.1. Under the elastic case, failure criteria is taken as bending stress higher than the yield strength of 35.2 MPa. Overall, the FEA models for the alternate designs showed an improvement of minimizing stress.

Table 4.1 CATIA V5 R20 FEA von Mises results summary including the result for the traditional 3 mm hinge from Gribbins and Steinhauer (2014) for comparison

Hinge Type	Hinge Length (mm)	Maximum von Mises Stress (MPa)
Traditional	3	32.2
	6	21.5
	12	14.1
ZigZag		12.3
Lamella	12	18.9
Wave		10.3

Comparing just the elongation effect within the traditional designs shows that longer hinge length results in lower, more evenly distributed stresses. While the traditional 3 mm type studied by Gribbins and Steinhauer (2014) experienced a maximum von Mises stress of 32.2 MPa, the 6 mm hinge length experienced 21.5 MPa and the 12 mm design experienced a maximum of 14.1 MPa. This is reasonable as there is more area for the stresses to be distributed over.

The zigzag and wave alternate designs increased the surface area within the same hinge length and resulted in even lower stresses of 12.3 MPa and 10.3 MPa. Designs that also offer multiple rotation points also distribute the stress as evident in the zigzag and wave designs compared to the traditional hinge design which concentrated the bending to a single large area at the end of the hinge and the lamella structure that concentration on the connection segments.

Conclusions and Future Work

The zigzag and wave hinge designs, which incorporate large surface area for the stress to distribute, show promise of a successful living hinge design for parts made of FDM ABS. While elongating the traditional hinge design reduces the maximum stress experienced by the hinge, alternate designs can achieve lower stresses with less hinge length. This is important if space is an important consideration and further extension of the hinge to achieve similar stress distribution is not feasible.

The wave design displayed the lowest von Mises maximum stress experienced on the hinge at 10.3 MPa. Comparing this with the yield strength of the material, 35.2 MPa, suggests that further deformation is possible making this design a possible candidate for a usable living hinge.

Refinement of the FEA case to include the effects of the horizontal displacement or utilize a rotational displacement is desired. Due to CATIA's V5 R20 linear computation limitations, alternate software would be necessary to analyze the stress distribution at an enforced deformation greater than 10°. Experimental analysis on the hinges is needed to validate the results of the FEA.

Future development on optimizing the alternate designs and exploring even more possibilities are greatly encouraged. Another area of interest would be testing the alternate designs with other types of materials and processes for feasibility as a usable living hinge.

References

Ahn, S.-H., Montero, M., Odell, D., Roundy, S., & Wright, P. K. (2002). Anisotropic material properties of fused deposition modeling ABS. *Rapid Prototyping Journal*, *8*(4), 248–257.

bart. (2008, November 19). *Creating hinges and moving parts*. *The Shapeways Blog*. Retrieved July 26, 2014, from /blog/archives/141-Creating-hinges-and-moving-parts.html

Elleithy, R. H. (2007). Plastic integral hinges; design, processing, and failure analysis. In *ANTEC 2007* (Vol. 5, pp. 2741–2744). Cincinnati, Ohio.

Gibson, I., Rosen, D. W., & Stucker, B. (2010). *Additive manufacturing technologies rapid prototyping to direct digital manufacturing*. New York; London: Springer. Retrieved from http://dx.doi.org/10.1007/978-1-4419-1120-9

Gonzalez, N., & Kerl, F.-J. (2008, April 15). *EOS Design Rules Design study: living hinge sintering*. Retrieved from http://www.rapidprototyping.nl/uploads/media/SLS_Design_study_living_hinge_02.pdf

Gribbins, C., & Steinhauer, H. M. (2014). Experimental analysis on an additively manufactured ABS living hinge. In *International Solid Freeform Fabrication Symposium An Additive Manufacturing Conference* (Vol. 2012). Austin, Texas: The University of Texas at Austin.

Hague, R., Mansour, S., & Saleh, N. (2004). Material and design considerations for Rapid Manufacturing. *International Journal of Production Research*, *42*(22), 4691–4708.

Hoffman, J. M. (2004, August 19). Care and feeding of living hinges. *Machine Design*, *76*(16), 64, 66.

Hopkinson, N., Hague, R. J. M., & Dickens, P. M. (2006). *Rapid manufacturing: an industrial revolution for the digital age*. Chichester, England: John Wiley.

Kim, H. S., Son, J. S., & Im, Y. T. (2003). Gate location design in injection molding of an automobile junction box with integral hinges. *Journal of Materials Processing Technology*, *140*, 110–115. doi:10.1016/S0924-0136(03)00700-3

Poli, C. (2001). *Design for manufacturing a structured approach*. Boston: Butterworth-Heinemann.

Stratasys, Ltd. (2013). Functional Prototyping - Living Hinges. Retrieved from http://www.stratasys.com/applications/functional-prototyping/living-hinges

Tres, P. A. (2000). *Designing Plastic Parts for Assembly* (4th ed.). Cincinnati: Hanser-Gardner.

whpthomas. (2012). *Ear Raft - Makerware Print Aid by whpthomas*. *Thingiverse*. Retrieved August 3, 2014, from https://www.thingiverse.com/thing:38272

Zamani, N. G. (2010). *CATIA V5 FEA tutorials: release 19*. Mission, KS: SDC Publications.

Chapter 5

Thesis Conclusion

Summary

This research investigated the implementation of living hinge designs utilizing the additive manufacturing process of fused deposition modeling. The study included initial numerical and analytical analyses, tensile testing to refine numerical analyses, and evaluation of dimensional accuracy of fabricated living hinges. Although the initial analytical approach indicated a successful elastic hinge, further experimental analysis is needed to support the findings of both the numerical and analytical solutions. The numerical analysis using CATIA V5 R20 resulted in the expected deformations, but indicated high stresses implied plastic behavior within the hinge. Due to CATIA's V5 R20 FEA linear computational limitations, accurate assessment of the possible plastic behavior within the hinge requires further experimental work for this particular living hinge design.

The tensile testing portion of the research resulted in an increase of the material property values as compared to previous literature, a yield strength of 28.6 MPa to 35.2 MPa, respectively. The characteristics of the stress-strain curve displayed brittle behavior that can be attributed to the high strain rate or the possibility of microvoids affecting the fracture toughness of the material. The software limitations of the MakerBot 2X required modification of the traditional living hinge for fabrication. Evaluation of the dimensional accuracy in the fabricated living hinges indicated a higher than expected shrinkage rate of the length geometry created in the X axis as well as the width geometry in the Z axis. Higher than nominal thickness values created in the Y axis suggest the minimal layer

fabrication thickness is around 0.9 mm. Adjustment of building parameters in the MakerBot software may result in closer to nominal dimensional values.

The investigation on alternate design geometry consisted of elongating the traditional design geometry followed by the exploration of alternate and complex living hinge geometry. Simply elongating the traditional hinge design resulted in an increased stress distribution over the hinge length although the center of rotation, the highest stress concentration, appeared to focus on the fixed end rather than the center of the hinge, as desired. The zigzag and wave alternate designs demonstrated smoother bending as indicated by the stress evenly distributed between the segments along the entire hinge rather than concentrated at the fixed end. The wave design had the lowest von Mises maximum stress of 10.3 MPa. This compared with the FDM ABS yield strength of 35.2 MPa suggests the potential for a successful living hinge design that behaves within the elastic region.

Limitations and Future Work

The results of this research indicate several possible areas for future work: conducting experimental application testing of living hinges, refining the finite element analysis, and optimizing alternate designs are suggested for future study.

Conduct Experimental Application Testing

Validity of the calculated bending stress from the numerical and analytical solutions is needed. The actual stress occurring within the living hinge during application can be assessed from an experimental analysis that observes the force necessary to displace the hinge.

Refine Finite Element Analysis

　　More accurate solutions of the stress distribution necessitates refinement of the FEA cases. This would consist of including the effects of the horizontal displacement along with the vertical displacement or utilizing a rotational displacement. Due to CATIA's V5 R20 linear computation limitations, alternate software would be necessary to analyze the stress distribution at an enforced displacement greater than the linear computational maximum of $10°$. Further investigation on obtaining the necessary values for classifying an anisotropic material property is also needed.

Optimize Alternate Designs

　　The research was largely limited by the use of predefined geometry dimensions as guided by previous living hinge research (I. Gibson, Goenka, Narasimhan, & Bhat, 2010). Future development on optimizing the dimensions of alternate living hinge designs and exploring other design geometries are suggested. Optimizing the design geometry can refer to either modification of the geometry to printer capabilities or application design goals.

　　Printer capability optimization requires understanding of MakerBot terminology for adjustment of build parameters under the advanced options menu as well as familiarity on how the modified parameters effect the resultant printed part. A common challenge with entry level printers, such as the MakerBot 2X, is consistency between prints. Application design goal optimization includes exploration on geometry that evenly distributes stress and encourages smooth, circular bending.

Conclusion

These three studies have established an initial investigation on applying living hinge designs in the fused deposition modeling process of additive manufacturing. The results can be used to provide insight in exploring alternate designs that may be better suited for additive manufacturing capabilities. In summary, this research provides several areas for exploration on designing for additive manufacturing processes.

Appendix A
Material Datasheet from CES EduPack 2013 (CES EduPack 2013, 2013)

CES 2013 EDUPACK

ABS (injection molding, platable)

Identification
Designation
Acrylonitrile Butadiene Styrene (Injection Molding, platable)

Tradenames
Abelac; Abifor; Abstron; Absylux; Acstyr; Akmaril; Alcom; Anjalin; Aplax; Arradur; Astalac; Athpol; Aurocril; Bapolan; Bulksam; Certene; Cevian; Claradex; Collimate; Compolac; Cycoele; Cycogel; Cycolac; Dafnelac; Denisab; Diapet; Diastat; Dynacom; Endura; Ensidur; Espree; Estadiene; Excelloy; Faradex; Farralloy; Fiberfil; Forsan; Hanalac; Highlac; Hiloy; Hylac; Isolac; Isopak; Kane Ace; Kapstone; Kralastic; Lastilac; Lupros; Lustran; Lustropak; Magnum; Nevies; Nilac; Novodur; Osstyrol; Palran; Perlac; Permastat; Plasfil; Polidux; POLYabs; Polyfabs; Polyflam; Polylac; Polyman; Porene; Pre-Elec; Remex; Retain; Ronfalin; Rotec; Santac; Senosan; Seracril; Shinko-lac; Sicoflex; Sinkral; Starex; Stylac; Superex; Tairilac; Taitalac; Tarodur; Tecaran; Techno; Tekral; Terblend; Terez; Terluran; Tomax; Toyolac; Toyolacparel; Triax; Tufbaria; Tynab; UplAxs; Ultrastyr; Umastyr; Unibrite; Vampsab; Whistatt

General Properties
Density	1.04e3	- 1.07e3	kg/m^3
Price	* 2.84	- 3.13	USD/kg

Composition overview
Composition (summary)
Block terpolymer of acrylonitrile (15-35%), butadiene (5-30%), and Styrene (40-60%).

Base	Polymer
Polymer class	Thermoplastic : amorphous
Polymer type	ABS
Polymer type full name	Acrylonitrile butadiene styrene
Filler type	Unfilled

Composition detail (polymers and natural materials)
Polymer	100	%

Mechanical properties
Young's modulus	2.21	- 2.62	GPa
Compressive modulus	* 2.21	- 2.62	GPa
Flexural modulus	2.34	- 2.68	GPa
Shear modulus	* 0.79	- 0.937	GPa
Bulk modulus	* 3.86	- 4.06	GPa
Poisson's ratio	* 0.391	- 0.407	
Shape factor	5.6		
Yield strength (elastic limit)	42	- 46	MPa
Tensile strength	42	- 46	MPa
Compressive strength	* 52.8	- 58.2	MPa
Flexural strength (modulus of rupture)	72.4	- 79.3	MPa
Elongation	* 15.3	- 20.9	% strain
Hardness - Vickers	* 13.2	- 14.6	HV
Hardness - Rockwell M	* 66	- 72	
Hardness - Rockwell R	103	- 109	
Fatigue strength at 10^7 cycles	* 14	- 18.2	MPa
Fracture toughness	1.9	- 2.1	MPa.m^0.5
Mechanical loss coefficient (tan delta)	* 0.0153	- 0.0181	

Impact properties
Impact strength, notched 23 °C	10.7	- 23.1	kJ/m^2
Impact strength, notched -30 °C	4.88	- 10.9	kJ/m^2

Values marked * are estimates.
No warranty is given for the accuracy of this data

Appendix B
Adapted Analytical Approach Algorithm (Tres, 2000)

Elastic Strain Evaluation

Select material

↓

Establish Hinge Thickness, L_1

↓

Establish Hinge Length

↓

Compute A

↓

IF — $L_1 > A$ → **Stop** Pure Elastic Bending

$L_1 < A$

↓

Plastic Strain Evaluation

Select Recess Depth

↓

Compute B

↓

$L_1 < B$ — IF — $L_1 > B$

Compute D   Compute C

$L_1 < D$ $L_1 > D$ $L_1 < C$ $L_1 > C$

Stop Failure ← IF → **Stop** Plastic Bending and Tension

Stop Failure ← IF → **Stop** Pure Plastic Bending
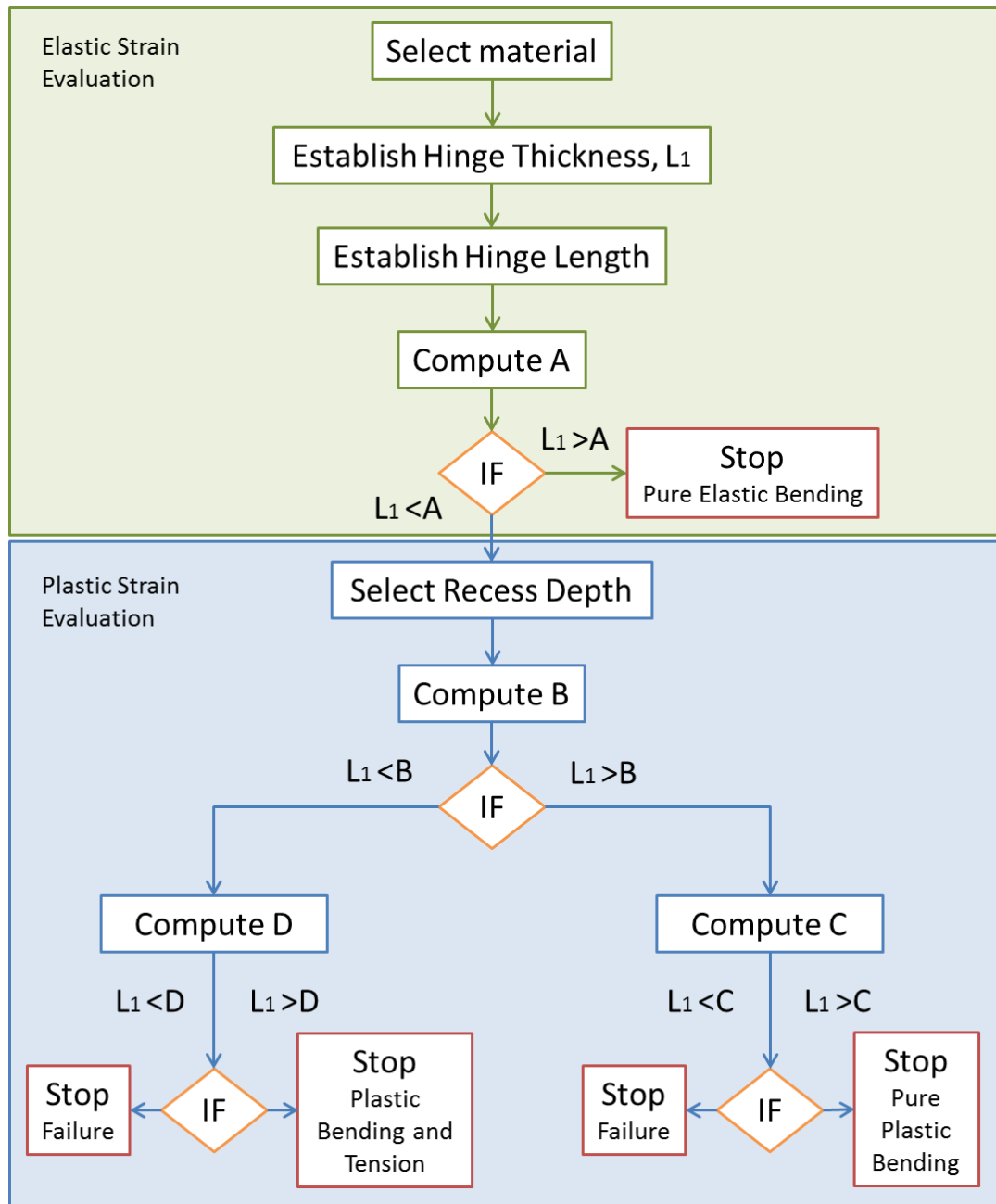
Conditions are the lower limits for the neutral axis with respect to case:
A: Elastic strain – Equation 2.6
B: Plastic bending strain (general) – Equation 2.7
C: Plastic bending strain (center of living hinge never reaches plastic deformation) – Equation 2.8
D: Mixture of plastic bending and tension strain (behaves like a viscoelastic material) – Equation 2.13

Appendix C
Analytical Approach MATLAB Code
Material Selection

```matlab
function [ mat_type, sigU, sigY, Esy, epsU, epsY, v ] = HingeMaterial( mat )
% Material data from CES Edupack
%
switch mat
%% Material Data

case 1
mat_type = 'ABS FDM Adjusted';

% Tensile strength at break (Pa)
sigU = 28.6*10^6;

% Tensile strength at yield (Pa)
sigY = 28.6*10^6;
%
% Secant modulus for the yield point (Pa)
Esy = 2415*10^6;
%
% Ultimate strain (% strain)
epsU = 18.1;
%
% Yield strain (% strain)
epsY = 18.1;
%
% Poisson's ratio
v = 0.399;

    otherwise
        fprintf('missing material data');
        return
end


end
```

```matlab
% Cassandra Gribbins
% Thesis - Living Hinge Design Geometry Calculations
%
% Source: Designing Plastic Parts for Assembly by Paul A. Tres
% 6th Edition pgs 194-198

%% Initializing variables

clear
clc

format shortEng

% User input: Material type
mat = input('What is the material type? \nEnter: \n  "1" for ABS min\n  "2" for ABS avg\n
"3" for ABS max\n');
if mat >= 1
    [ mat_type, sigU, sigY, Esy, epsU, epsY, v ] = HingeMaterial( mat );
else
    fprintf('invalid material selection\n');
    return
end

% User input: Hinge Thickness
t = input('\nWhat is the hinge thickness (mm)?\n');
if t <= 0
    fprintf('invalid hinge thickness\n');
    return
end

% User input: Hinge Length
Y = input('\nWhat is the hinge length (mm)?\n');
if Y <= 0
    fprintf('invalid hinge length\n');
    return
end

% User input: Hinge Recess
Z = input('\nWhat is the hinge recess (mm)? Default 1 mm\n');
if Z < 0
    fprintf('invalid hinge length\n');
    return
end

% User input: Closing Angle
angledeg = input('\nWhat is the closing angle (deg)?\n');
if angledeg < 0
    fprintf('invalid hinge length\n');
    return
else
angrelad = degtorad(angledeg);
```

```matlab
end

% Min processing thickness, X
X = 2*t;


%% Evaluation if PURE ELASTIC hinge

% Compute A (Condition to have elastic strain only for a min length
%   of the fiber along the neutral axis Eq. 7.9 pg 183)
A = (anglerad*t*Esy)/(sigY);

% IF pure elastic hinge (Y>A) stop
if Y>=A
    %      hinge angle
    phi = (Y*sigY)/(t*Esy);
    %      hinge radius
    R = (t*Esy)/sigY;

    fprintf('\nUser Input Variables:\nHinge Thickness, t %d mm',t);
    fprintf('\nHinge Length, Y %d mm\nHinge Recess, Z %d mm\n',Y, Z);
    fprintf('\nPure elastic hinge - no failure\n');
    fprintf('\nY>A\nCondition to have elastic strain \nonly for a minimum length of the↙
fiber \nalong the neutral axis A %d< Y %d mm',A,Y);
    fprintf('Maximum hinge strain, %d percent strain\n',epsU);
    fprintf('Calculated variables:\nHinge angle (<pi for pure elastic strain), phi %d↙
(deg)\nHinge radius, R %d(mm)\n',phi,R);
    return
end

% ELSE (Y<A) continue

%% Evaluation if PURE PLASTIC hinge

% Compute B (Lower limit of length of neutral axis L1 for the pure bending
%   region Eq. 7.17 pg 185)
B = anglerad*(t+Z);

% IF Y>B - Pure Plastic Bending
if Y>=B
    %    Compute C (Below lower limit, B, living hinge behaves like
    %    a visco-elastic material. Consider a tension strain that models the
    %    necking effect Eq. 7.18 pg 185)
    C = (anglerad*t)/epsU;
    Cu = C;
    Cy = (anglerad*t)/(epsY);
%    Y>C No Failure, stop
    if Y>=C
    fprintf('\nUser Input Variables:\nHinge Thickness, t %d mm',t);
    fprintf('\nHinge Length, Y %d mm\nHinge Recess, Z %d mm\n',Y, Z);
    fprintf('\nPure plastic bending\n');
```

```matlab
    fprintf('\nY<A\nCondition to have elastic strain only for a minimum length\n of the ↙
fiber along the neutral axis \nY %d < A %d mm\n',Y,A);
    fprintf('\nY>B\nCondition for pure bending strain above lower limit: \nY %d > B %↙
dmm\n',Y,B);
    fprintf('\nY>C\nCondition that length is above visco-elastic material limit (near↙
lower limit):\nY %d > C %d mm\n',Y,C);
    %      hinge angle
    phi = (Y*sigY)/(t*Esy);
    %      hinge radius
    R = (t*Esy)/sigY;
    fprintf('\nCalculated variables:\nHinge angle, phi %d(deg)\nHinge radius, R %d(mm) ↙
\n',phi,R);
    fprintf('\nMaximum hinge strain, %d percent strain\n',epsU);

    fprintf('\nY>Cy\nCheck if there is failure when using yield:\n');
    if Y<=Cy
        fprintf('Hinge failure over yield\n');
        fprintf('Y %d < Cy %d\n',Y,Cy);
    end
    fprintf('No failure over yield\n');
    fprintf('Y %d > Cy %d\n',Y,Cy);
    return
%    Y<C Failure
    else

        fprintf('Hinge Failure\nY %d < A %d\n',Y,A);
        fprintf('Y %d > B %d \n',Y,B);
        fprintf('Y %d < C %d',Y,C);
        fprintf('\nUser Input Variables:\nHinge Thickness, t %d mm',t);
        fprintf('\nHinge Length, Y %d mm\nHinge Recess, Z %d mm\n',Y, Z);
        return
    end
end
% ELSE (Y<B - Mixture of plastic bending and tension)
% continue
%
%% Evaluation if plastic tension and bending
% Compute D (smallest living hinge length Eq. 7.77 pg 193)
D = (anglerad*v*(X+Z))/(v+2*(1-sqrt(1-v*epsU)));

% IF Y>D no failure
if Y>D
%   Calculate elastic strain portion Wp Eq. 7.90 pg 197
Wp = (Y*sigY)*(2*pi*Esy);

% Calculate new thickness U Eq. 7.92 using length neutral axis Eq. 7.18 and tension↙
strain Eq. 7.59
    C = (pi*t)/(4*epsU);
    Cu = C;
    Cy = (pi*t)/(4*epsY);
L1 = C;
```

```
l = Z;
epsT = (pi/L1)*(t+l)-1;
U = t*(1-v*epsT);

% Bending strain Eq. 7.93
epsB = ((pi*t)/(Y^2))*(Y*(1+v)-(pi*v)*(t+Z));

% Neutral axis shift Eq. 7.94
V = (Y/pi)+(v*t)-l-((pi*v*t^2)/Y)-((pi*v*t*l)/Y);

% Elastic strain Eq. 7.95 using h (distance from the inside fibre to the
% neutral axis under the plastic bending and tension Eq. 7.52
h = (L1/pi)-l-((v*t)/L1)*(pi*t+pi*l-L1);
% W = ((2*((2*t)*(1-v*epsT))-h)*sigY)/((pi*t*(2-v*epsT+l)-Y)*E);
%      hinge angle
phi = (Y*sigY)/(t*Esy);
%      hinge radius
R = (t*Esy)/sigY;

fprintf('\nUser Input Variables:\nHinge Thickness, t %d mm',t);
fprintf('\nHinge Length, Y %d mm\nHinge Recess, Z %d mm\n',Y, Z);
fprintf('\nPlastic strain due to mixture of bending and tension\n');
fprintf('\nY>D\nCondition is greater than smallest living hinge length: Y %d >D %dmm\n', ↙
Y,D);
fprintf('\nCalculated variables:\nHinge angle, phi %d(deg)\nHinge radius, R %d(mm)\n', ↙
phi,R);
fprintf('Maximum hinge strain, %d percent strain\n',epsU);
fprintf('Elastic strain portion, Wp %d \n',Wp);
fprintf('\nCalculated variables:\nNew hinge thickness, U %d mm\nBending strain, epsB %↙
d\n',U,epsB);
fprintf('\nNeutral axis shift/Distance from inside fiber to \nneutral axis under plastic↙
bending and tension, h %d \n',h);
fprintf('If h is negative, the tensile strain \nreaches high values - under tension');
fprintf('\nthere is no neutral axis within the living hinge thickness\n');

    % Else (Y<D) Failure
    else
        fprintf('Hinge Failure');
        fprintf('\nUser Input Variables:\nHinge Thickness, t %d mm',t);
        fprintf('\nHinge Length, Y %d mm\nHinge Recess, Z %d mm\n',Y, Z);
        return
end
```
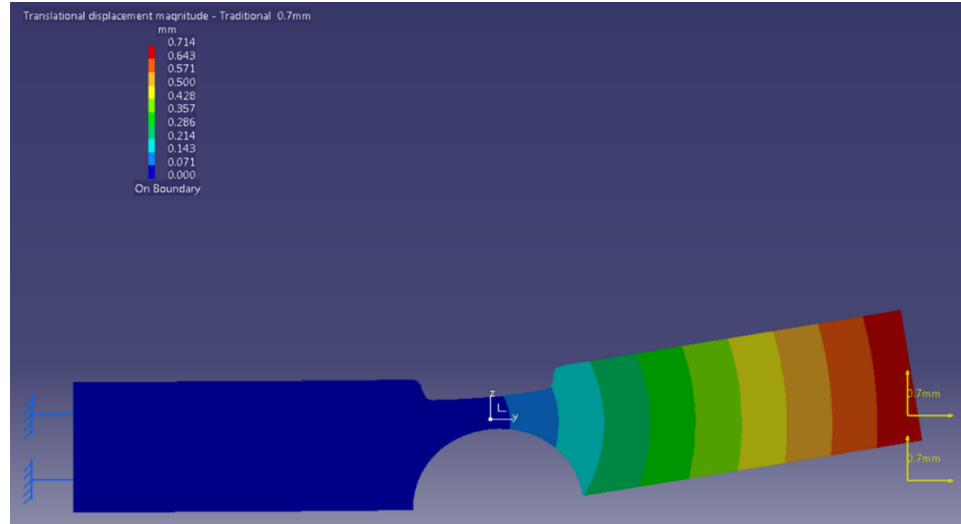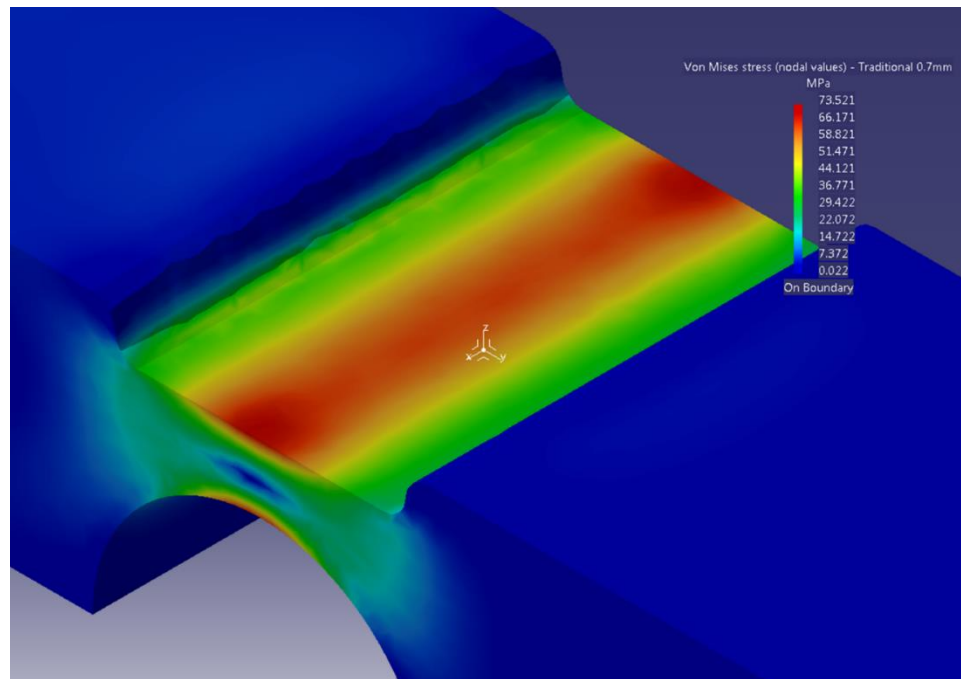
Appendix E
Traditional PP Design Geometry
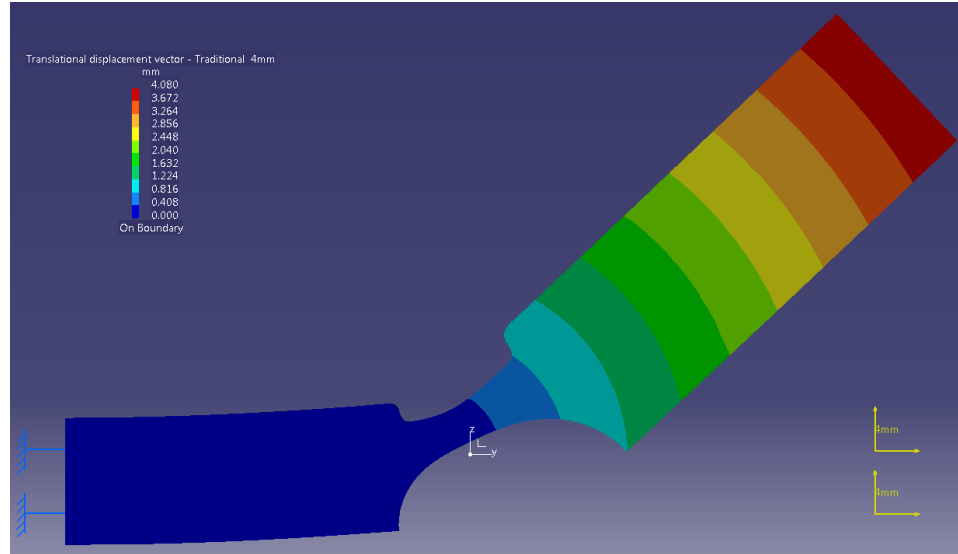## Results from CATIA V5 R20 for Enforced Displacement of 0.7 mm

Figure E-1 Translational displacement vector diagram for enforced displacement 0.7 mm on traditional PP design geometry
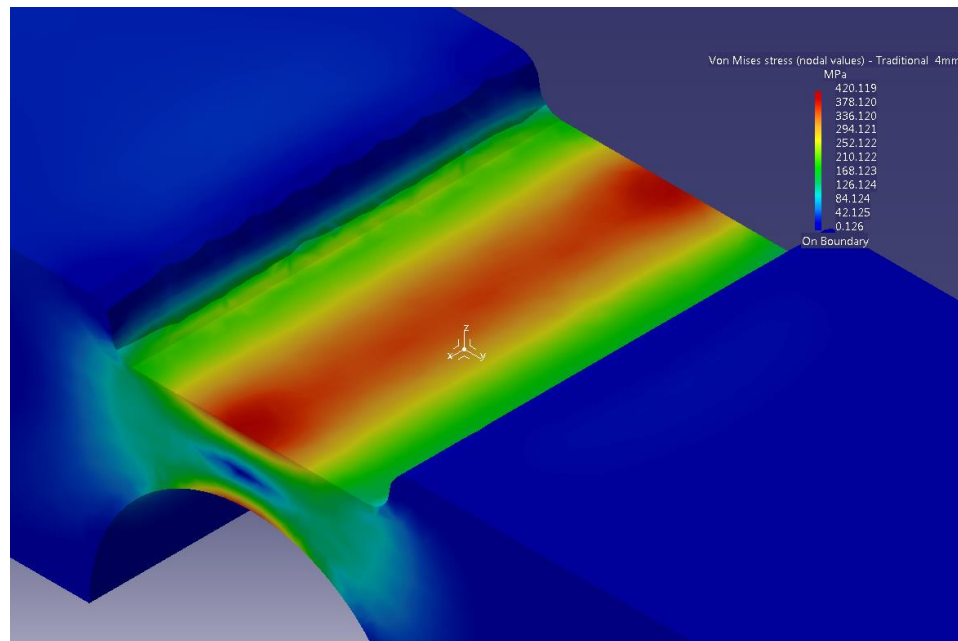

Figure E-2 von Mises stress diagram for enforced displacement 0.7 mm on traditional PP design geometry

Appendix F
Traditional PP Design Geometry
## Results from CATIA V5 R20 for Enforced Displacement of 4.0 mm

Figure F-1 Translational displacement vector diagram for enforced displacement 4.0 mm on traditional PP design geometry
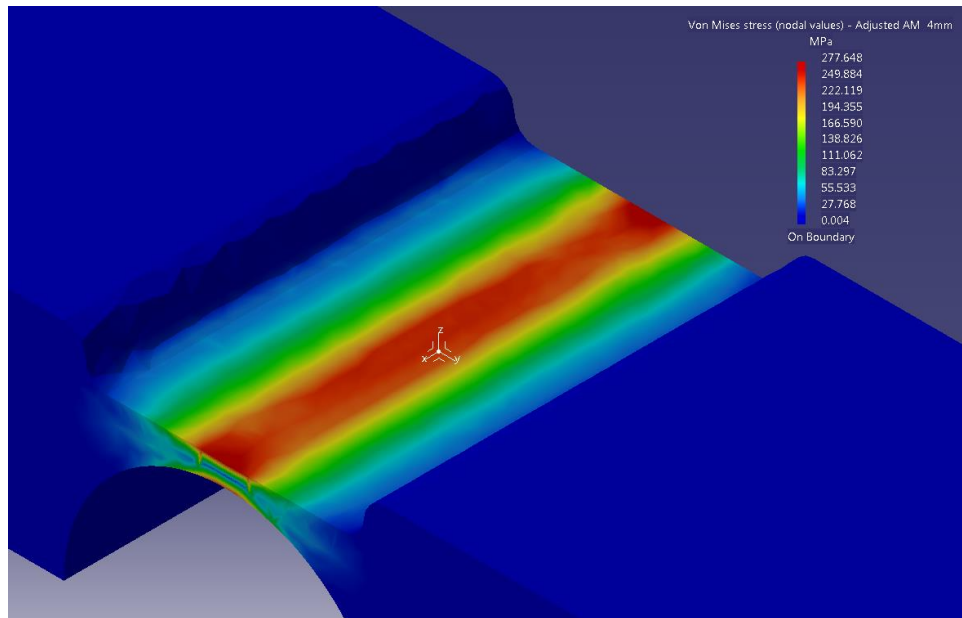

Figure F-2 von Mises stress diagram for enforced displacement 4.0 mm on traditional PP design geometry

Appendix G
Adjusted AM Design Geometry
Results from CATIA V5 R20 for Enforced Displacement of 0.7 mm and 4.0 mm
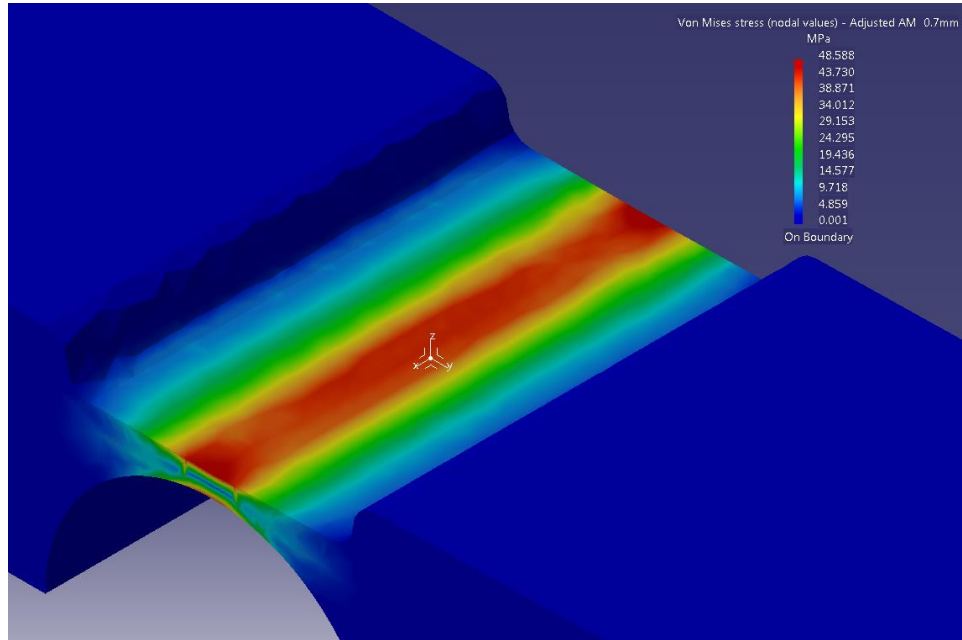
Figure G-1 von Mises stress diagram for enforced displacement 0.7 mm on adjusted AM design geometry

Figure G-2 von Mises stress diagram for enforced displacement 4.0 mm on adjusted AM design geometry